Investigating North Greenland ice shelves and their response to warming climate

Alice Hoyle

Scott Polar Research Institute

Newnham College, University of Cambridge

Submission for Master of Philosophy in Polar Studies

2020-2021

Table of Contents

List of Figures

List of Tables

Acknowledgements

This thesis was researched and written during an exceptional time in global history, and its completion would not have been possible without the help of some equally exceptional people. Firstly, and most importantly, I would like to thank the supervisor of this project - Poul Christoffersen. For his outstanding dedication in providing guidance to his students, patience throughout countless technical difficulties, and calm and thoughtful words of encouragement, I am extremely grateful. Secondly, an essential part of any postgraduate work is peer collaboration, and I could not have asked for a more encouraging or intelligent partner in this degree than Holly O'Neill.

This thesis has built on the work of many talented academics. This includes the work of Tom Cowton, whose detailed publications served as the model for this thesis' methodology, and whose excellent advice was essential to developing this thesis. I would also like to thank James Lea for his assistance with automated analysis of digitised terminus positions. TJ Young has been exceptionally helpful to this project in helping to source runoff reanalysis data, as has Brice Noel and the team at Utrecht for allowing access to their model outputs. I thank the wider community at SPRI, from whom generous advice and support has always been available. Most notably, this includes Frazer Christie, who replied to continuous dull technical questions with unending enthusiasm for the possibilities of Matlab and provided code which was used as the template for oceanographic analysis.

Finally, I would like to thank my family – who having believed they had finally handed me off for good to postgraduate study, welcomed me back to complete the bulk of this dissertation from home during the third Covid-19 lockdown. None of my achievements, in particular this dissertation, would have been possible without their support.

Declaration

I certify that this essay/dissertation is the result of my own work and includes nothing which is the outcome of work done in collaboration except where specifically indicated in the text.

I declare the word count does not exceed the 20,000-word limit excluding introductory pages, figure captions, reference list and appendices.

25th June 2021

Abstract

The Greenland Ice Sheet has been losing mass at an increasingly rapid pace since the mid 1990s, which is forecast to accelerate further into the coming century. This mass loss is translated directly into global mean sea level rise, with severe consequences for coastal communities around the world who will rely on accurate predictions of sea level contributions to prepare for and mitigate the resultant effects. A significant source of uncertainty in models which predict sea level rise is the response of ice shelves and their grounding lines to environmental forcing. Ice shelves are critical components to understand because they exert a buttressing effect on upstream ice, preventing it from discharging rapidly to the ocean through exerting a back stress on glaciers which would otherwise be free to accelerate, thin, and increase output of mass to the ocean in response to a warming climate. This study quantified changes to ice shelf areas in North Greenland between 1995 and 2016 with the aim of understanding vulnerability to increasing ocean temperature and ice shelf runoff in the region. This was achieved through the measurement of annual average terminus position through repeat digitisation of ice shelf margins in GEEDiT, a tool developed by Lea (2018), which were then integrated with linearly interpolated grounding lines from the ESA's Climate Change Initiative project, which measured grounding line positions in the late 1990s and 2017 across North Greenland. The ice shelf areas of Petermann Gletsjer, Ryder Gletsjer, Hagen Brae and Nioghalvfjerdbræ were found to have changed by -27%, -8%, +28%, and +180% respectively. A secondary aim was to understand whether a linear relationship between environmental forcing variables and terminus positions exists at these ice shelves, which has previously been identified by Cowton et al. (2018) at tidewater glaciers. It was established that a direct linear co-integration is not applicable to ice shelf environments, which consequently increases concern that current approximations of linear forcing used in sea level predictions are severely limited. This is because local geometry and bathymetry play a strong role in modulating the delivery of heat to ice shelf environments.

1. Introduction

1.1 Motivation for study:

From 1992 to 2018, the Greenland Ice Sheet (GrIS) lost between 3400 and 4200 billion tonnes of ice, resulting in an increase to global mean sea level of more than 10 mm (The IMBIE Team, 2020). Recent estimates of surface mass balance indicate that total mass output has increased sixfold from estimates of output in the 1980s, in response to global warming trends in the ocean and atmosphere (Mouginot, et al., 2019). 52% of this mass was lost via direct melt of the ice sheet resulting in increased runoff, and 48% was caused by enhanced rates of glacial discharge (The IMBIE Team, 2020). Throughout this period, interdecadal rates of mass loss have been variable: increasing rapidly throughout the early 2000s from an approximately steady state in the 1990s (average of 18 ± 28 Gt a^{-1} between 1992 and 1997) to a maximum of 270 ± 27 Gt a^{-1} (2007-2012). Mass loss then slowed slightly to an average of 217 ± 32 billion t a^{-1} (2013-2017) as shifting phases of the NAO added variability in atmospheric temperatures (The IMBIE Team, 2020).

Low-lying coastal communities around the globe are already feeling the effects of rapidly rising sea levels and having to adapt infrastructure to cope with increasing chances of flooding (Esteban, et al., 2020). If current predictions of sea level rise in the coming decades hold true, every five years the odds of extreme flooding in coastal regions will double (Taherkhani, et al., 2020). With 230 million people located on land below 1 metres above sea level (henceforth m.a.s.l. or m.b.s.l. – metres below sea level) (Kulp & Strauss, 2019), it is of vital importance that modellers can predict the rate at which the GrIS will continue to contribute to sea level rise in coming decades. Models used to establish these predictions are hampered by uncertainties of up to 55% in upper-level emissions scenarios (Goelzer, et al., 2020), a large portion of which is caused by poor understanding of the relationships between environmental forcing factors and the edges of ice sheets, where ice shelves buffer mass lost to the ocean through a buttressing effect. This is particularly true of calving events from the ice

shelf, which are not well represented in models (Pattyn, et al., 2017). Across Greenland, the north and north-easterly regions, which together hold 2.7 m of equivalent sea level rise in ice volume, are considered to have the most potential for contribution to sea level rise in the future. This is because buttressing ice shelves remain in this region; the removal of which could increase currently slow ice velocities and associated discharge to the ocean (Mouginot, et al., 2019). Quantification of the potential loss through de-buttressing is challenging, as limited in situ data exists from the most northerly and therefore remote part of Greenland to use in hindcasting exercises (Orsi, et al., 2017).

Current models, including ISMIP6 – used to inform the IPCC's sea level rise projections – assume linear relationships between terminus position and ocean temperature (Nowicki, et al., 2016). Wood et al. (2021), as well as many workers in the field of glacial geometry suggest that these assumptions may not hold water when applied to more variable environments, including ice shelves, because of the highly localised factors of geometry and bathymetry disrupting regional averages, as well as positive feedbacks of melt undercutting being initiated in regions which might otherwise be considered dynamically stable. Additionally, localised grounding line migrations forced by warm ocean waters and controlled by fjord topography is not included in modelling studies (An, et al., 2021), but has the potential to induce changes to the dynamics at the margins of vulnerable ice sheets.

Linear relationships have been established in other areas of Greenland by Cowton et al. (2018), Slater et al. (2019), and Fahrner et al. (2021) at marine terminating glaciers but are yet to be established at glaciers with ice shelves. It is undoubtedly of great importance to establish whether the linear relationships considered by these authors hold fast across variable environments of the Greenland Ice Sheet, as if this simplified relationship is applicable at complex environments over long timescales, uncertainty associated with long-term predictions of mass loss can be reduced. Greenland is an important study site in its own right, but any improved insight into ice shelf behaviour is also important for assessing Antarctic dynamics, which are

strongly influenced by the ice shelves surrounding much of its coast. Antarctic ice shelves are responsible for buffering the discharge of ice volumes an order of magnitude greater than in Greenland, but are not yet subject to the same degree of warming which Greenland is currently undergoing.

1.2 Aims and Objectives:

The overarching first aim of this study is to quantify the areas of North Greenland ice shelves, in order to understand their vulnerability to increases in regional ocean temperature and ice sheet runoff over the last several decades. The second aim is to understand whether a linear relationship previously identified between environmental forcing factors and terminus migration at grounded tidewater glacier margins can be extended to also include glaciers with ice shelves at their termini. The specific objectives of this study are therefore as follows:

1. Generate inventory of North Greenland ice shelf areas over study period of 1995-2017:
    a. Obtain annual grounding line positions of glaciers through interpolation of InSAR measurements.
    b. Measure average annual calving front positions of glaciers through repeat digitisation of satellite imagery.

2. Measure variation in environmental forcing factors over the study period at each study site:
    a. Extract average annual surface and deep ocean temperatures from ensemble model of ocean conditions.
    b. Extract average annual cumulative runoff from RACMO model.

3. Assess evolving ice shelf dynamics in conjunction with ocean and atmospheric forcing data

a. Test Cowton, et al.'s (2018) linear response framework for tidewater glaciers to glaciers with an ice shelf component.
b. Consider how geometry or other locally variable factors may be modulating any non-linear aspect of the glacial response to environmental forcing at each site.

1.3 Study area

The study sites were determined by identifying glaciers along the North Greenland coast with large catchment areas, and intact ice shelves which remained in place year-round. From these glaciers, four sites were selected at regular intervals along the northern coast, to provide as much variation in local climate as possible within the study. The four study sites chosen, listed from northwest to northeast, are Petermann Gletsjer, Ryder Gletsjer, Hagen Brae, and Nioghalvfjerdsbræ. A map of the study site catchment areas, locations from where samples of ocean temperature were obtained, and centrelines of the ice shelves is displayed in Figure 7.

1.4 Structure

Having outlined the motivation for and principles of the study above, this thesis will go on to describe the contextual literature previously written in this field of study and previous work undertaken at the study sites in Chapter 2. Chapter 3 will explain how primary data used in this thesis was collected and detail the sources of secondary data, before Chapter 4 outlines the results of these investigations. This entails descriptions of how both ice shelf properties and environmental conditions have changed over the course of the study period, as well as the results of statistical testing for relationships between these variables and average annual terminus position. Chapter 5 discusses the implications of these results and how they relate to the aims outlined above, and reflects on the consequences of the findings within the context of wider literature and work in the field. Chapter 6 summarises the main findings of the study and the conclusions which can be drawn from them.

2. Literature Review

2.1 Polar ice shelves:

Ice shelves are floating masses of ice which remain attached to upstream grounded ice. They often occur on the fringes of ice sheets and caps, where outlet glaciers meet the ocean and begin to float at their terminus (Dowdeswell & Jeffries, 2017; Shabtaie & Bentley, 1987). Unlike ice tongues, which form seasonally at the terminus of many Greenlandic outlet glaciers (Moyer, et al., 2019), ice shelves are intact year-round, and can thus be considered permanent and dynamic components of the glaciers at which they occur (Minchew, et al., 2018). Glaciers transition into ice shelves at a point called the grounding line, where the terminus of the glacier is less dense than the surrounding ocean and so lifts from the bed, becoming ungrounded (Friedl, et al., 2018; Fricker, et al., 2002). The structure of an ice shelf is detailed in Figure 1, which shows the grounding line and calving front (or terminus). It also shows several proxies which can be used to locate the grounding line, including the break-in-slope (I), and landward limit of tidally induced ice shelf flexure (F) (see section 3.1.2 for more detail).

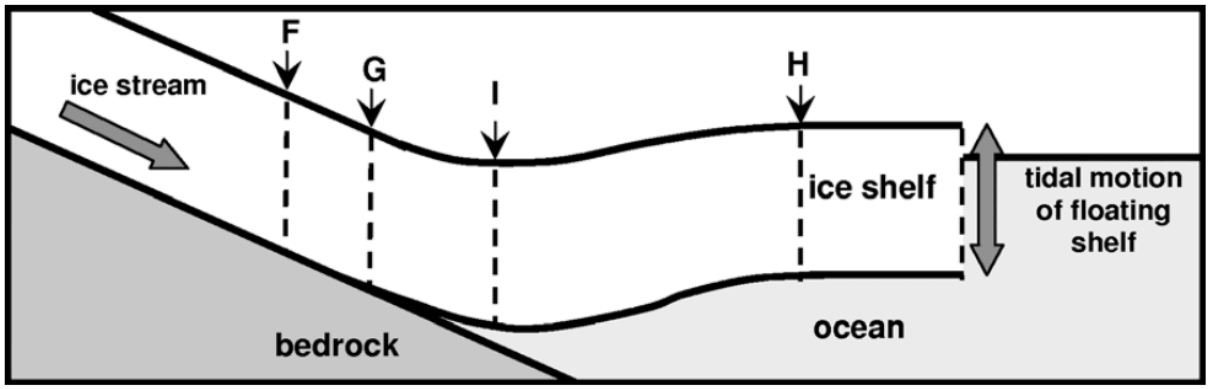

Figure 1: *Grounding zone anatomy diagram from Fricker and Padman (2006), adapted from Vaughan (1994).*

Antarctic ice shelves surround 55% of the Antarctic coastline (Dowdeswell & Jeffries, 2017), the largest of which (Ross and Filchner-Ronne) exceed 400,000 km^2 in area. Cyclical behaviour has been observed at these ice shelves throughout the 20th and 21st century, in which the ice shelves will gradually grow in area before calving large, tabular icebergs, losing area, and then begin to slowly grow back to their original pre-

calving size (Fricker, et al., 2009**;** De Rydt, et al., 2019)**.** However, these naturally occurring calving cycles in operation at some Antarctic glaciers have been disrupted by extensive ice shelf break up in the late 20th and early 21st centuries. Notably, this includes the break-up of Larsen B, which is thought to have been induced by ice shelf flexure caused by rapid synchronous supraglacial lake drainage (Banwell, et al., 2013). Joughin and MacAyeal (2005) found that natural calving cycles, or 'background' calving events to be primarily caused by internal glaciological stresses, rather than external oceanographic and atmospheric calving. They note a distinction between these natural cycles and the warming-triggered break-up of Larsen B.

A much smaller number of ice shelves are present in the warmer Northern hemisphere; Artic ice shelves exist only along the coasts of North Greenland, Ellesmere Island in Canada, and at some outlets along the coasts of Severnaya Zemlya and Franz Josef Land (Dowdeswell, 2017). Arctic ice shelves are much smaller than those in the Antarctic, reaching a maximum size of 400 km^2, or about 0.1% of the largest Antarctic shelf (Antoniades, et al., 2011). Arctic glaciers have been subject to widespread collapse over the last several decades, with the Milne ice shelf, located on the northerly coast of Ellesmere Island and previously Canada's last remaining ice shelf, collapsing in 2020, (Vincent & Mueller, 2020).

Whilst mass loss from ice shelves does not directly contribute to rising sea levels as they are in a continual state of floatation and thus displacing sea water already, their permanent attachment to grounded ice means they are capable of exerting influence on the discharge of glacial ice to the ocean through a buttressing effect (Holland, et al., 2020). Ice shelves, especially along the coast of Greenland, are contained within fjords, and are supported by valley walls. In turn, they exert a backstress on upstream ice, slowing the velocity of ice towards the ocean (Gudmundsson, 2019). Modelling and observational studies have found that if the ice shelves were to be removed or lose significant portions of their mass, de-buttressing would occur, and outlet glaciers around the polar ice sheets would accelerate and thin, resulting in disintegration of the West Antarctic Ice Sheet (Pattyn, 2017). De-

buttressing can occur both through the thinning of ice shelves (Gudmundsson, 2019), and following catastrophic loss of area during major calving events (Arthur, et al., 2021). Additionally, the retreat of ice shelf grounding lines or complete collapse of ice shelves has been hypothesised to play a role in initiating 'marine ice sheet instability' (MISI). This is a positive feedback process by which de-buttressing of marine ice sheets with retrograde grounding lines may lead to an exponential increase in mass loss, as grounding line retreat accelerates, and warming ocean waters bathe the interiors of the polar ice sheets inducing further retreat (Weertman, 1974; Schoof, 2007; DeConto & Pollard, 2016).

Ice shelves are clearly environments which have shown vulnerability to anthropogenic warming and have the potential to induce major changes to wider ice sheet dynamics. However, modelling projections of their future behaviour has proven difficult due to lack of understanding of the processes governing their behaviour, and limitations of coupling large scale ice sheet models with global ocean circulation models.

2.2 Environmental influence on ice shelves:

The behaviour of ice shelves may be influenced by many factors, several of which are climatological such as ocean and air temperatures. Increases in air temperature can induce mass loss from ice shelves by several mechanisms. Firstly, they contribute to the thinning of ice shelves directly through enhancing melt from the surface of the shelf (Washam, et al., 2019). Enderlin, et al. (2014) found 84% of Greenland's mass loss to be directly attributable to increased runoff. Increasing atmospheric temperatures can also lead to enhanced calving from ice shelves as meltwater which ponds on the surface weakens the internal structure of the ice shelf through the exertion of a load onto the glacier resulting in extensive hydrofracture (Scambos, et al., 2009). Warmth from increasing air temperature can therefore be considered as being transferred to the shelves via melt which forms runoff, and pools in supraglacial lakes (Banwell, et

al., 2014). The enhanced runoff generated by increasing air temperatures also enhances ice shelf mass loss through decreasing albedo of the surface (Lenaerts, et al., 2017), although both this mechanism and the weakening of the ice shelf structure will only occur if melt is not efficiently drained from the surface of the shelf to the ocean. Finally, enhanced surface runoff from atmospheric temperature increase can lead to the generation of melt plumes in the fjord waters in front of the ice shelf. This process occurs when glacial meltwater is exported to the ocean at deep points within the fjord, often close to or at the grounding line (Hewitt, 2020), and is thought to occur at both Greenlandic and Antarctic glaciers (van Dongen, et al., 2020; Moyer, et al., 2019; Holland, et al., 2007). The water discharged from the glaciers is cold and buoyant, and so lifts to the surface of the fjord waters, adjacent to the calving front of the tidewater glacier or terminus. The plume brings with it warm fjord waters with a resultant potential to increase melt rates at the ice shelf terminus through enhancement of fjord circulation (Christoffersen, et al., 2012). This process is illustrated in Figure 2.

Whilst air temperature has been shown to have an important role in governing ice shelf behaviour, the relationship established between oceanographic factors and ice shelf evolution has been found to be even more significant in both Antarctica and Greenland (Cook, et al., 2016; Straneo & Heimbach, 2013). Increases to ocean temperature induce mass loss directly through thinning in much the same way as air temperatures thin from above, as warmer temperatures generate enhanced rates of basal melt (Adusumilli, et al., 2020). This has been found to be a particular problem in West Antarctic, where basal melt induced by warming water in cavities below ice shelves is responsible for over 30% of the ice sheet's total output (Smith, et al., 2020). Increasing ocean temperatures are also thought to be increasing the rate of calving from ice shelves through thinning, and subsequent weakening of ice shelf integrity (Liu, et al., 2015; Benn, et al., 2017). In addition to this indirect mechanism of calving enhancement, work from Bassis and Ma (2015) implies that calving rates from ice shelves are also directly influenced by ocean forcing. Their numerical modelling studies found that enhanced melt within small basal crevasses can initiate instabilities

within the ice which allows for an increase in the height of fracture propagation throughout the ice shelf.

An additional mechanism by which warming ocean temperature enhances mass loss from ice shelves is through driving retreat of the grounding line. At the Zachariæ Isstrøm glacier in Greenland, Mouginot et al. (2015) attribute 7 km of grounding line retreat in 20 years to increasing ocean temperatures, and particularly to the increased inclusion of warmer Atlantic Waters (AW) within the underlying fjord. West Antarctic glaciers have been in a similarly alarming trend of grounding line retreat since the early 1990s (Rignot, et al., 2014), which is thought also to be primarily influenced by ocean forcing (Lowry, et al., 2019). Comparatively to increases in basal melt loss, ocean-induced grounding line retreat may have the potential to lead to more catastrophic mass from ice sheets as whole entities. This is because when the potential for MISI initiation through grounding line retreat is considered, this mode of ice shelf change has the most potential to disrupt the regimes of inland ice, rather than just local ice shelves (Goldberg, et al., 2009).

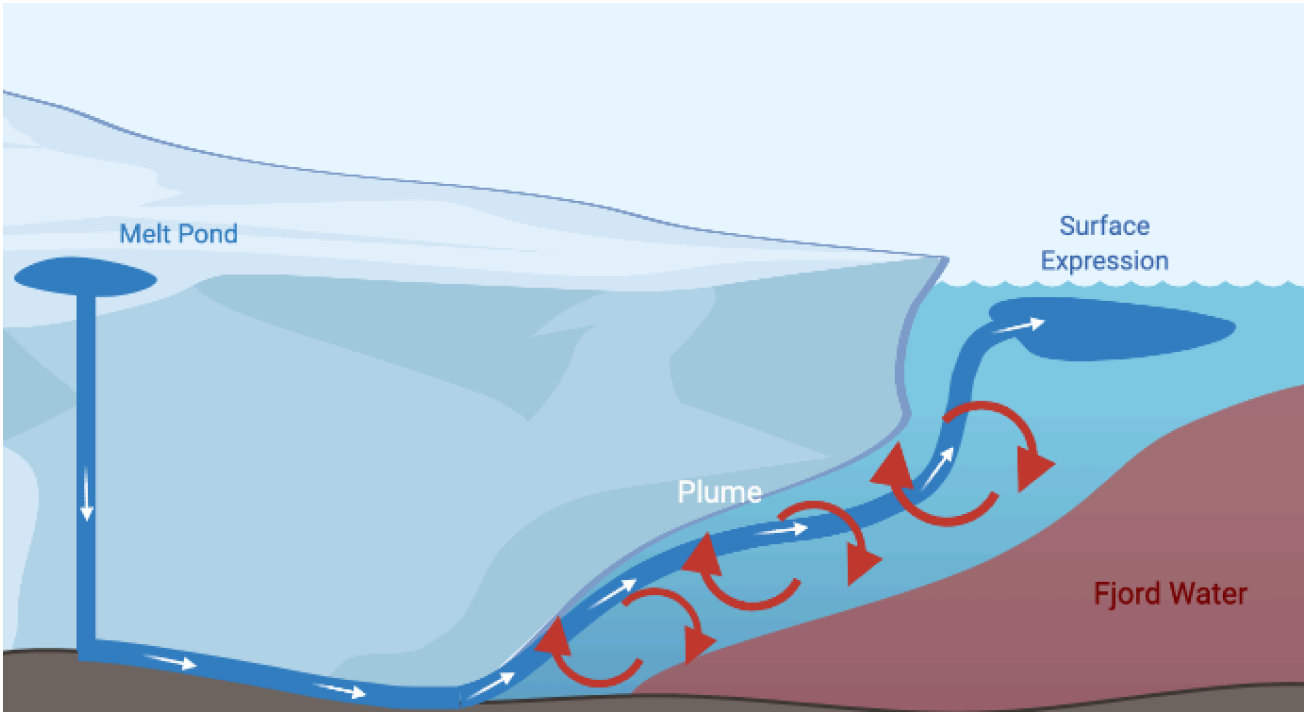

Figure 2: *Simplified diagram showing subglacial plume generation and subsequent entrainment of warm fjord water, from Barrett* (2020)*, developed from McConnochie et al.* (2020).

2.3 Glacial and bathymetric geometry:

The 'geometry' of glaciers and of the fjords within which they sit refers to the spatial properties of their bathymetry, topography, and characteristics such as width. It has an extremely significant effect on ice shelf behaviour, as it governs the frictional stresses which act on the ice shelf and its grounding line and can therefore either enhance response to environmental forcing factors or help stabilise the glacier and ice shelf (Porter, et al., 2014). A primary example of this is the presence of pinning points, which are topographic highs in a fjord or embayment's bed, whose frictional effect on the overlying ice induces a stabilising back stress and buttresses the upstream ice (Favier, et al., 2016). The geometry of the fjord in which a glacier rests also influences the properties of the water which reaches the grounding line (Eisermann, et al., 2020). In Antarctica, warm circumpolar deep water (CDW) is blocked from bathing the ice shelves of Dronning Maud Land Glacier by bathymetric high points called sills at the entrance to the fjords. These are common features which are created when glaciers sit in one position for an extended period and form an overdeepening through locally concentrated erosion, the sill of which is located at the glacier's frontal position during the time over which it remains stationary (Patton, et al., 2016). The same features have been found to prevent warm AW intrusions to the fronts of some glaciers in southeast Greenland (Millan, et al., 2018).

The geometry of glaciers also influences the structure of meltwater plumes. Carroll et al. (2016) found that a significant factor in controlling the effectiveness of plume induced melt is the depth of the grounding line below sea level. The deeper the grounding line, the warmer and saltier the resultant plume is, meaning that the undercutting potential associated with the plume is greater. In contrast, cool, fresh plumes at shallow grounding lines were found to cause more glacial degradation at the top of the water column. In addition to the depth at which plumes are initiated, plume location along the width of the glacier also impacts on the effectiveness of submarine melt, with plumes located close to the fjord walls capable of destabilising

the whole calving front due to interference with the resistive stresses at play in these regions of the terminus (Cowton, et al., 2019).

Geometry is thought to be responsible for some heterogeneity which has been observed in the polar outlet glacier responses to environmental forcing factors (Felikson, et al., 2017). Catania et al. (2018) found overdeepenings to cause the acceleration of terminus retreat, even in cases where the overdeepening primarily slope towards the ocean rather than inland, conditions which would normally be associated with stable or slow terminus retreat. They note that even deep but narrow channels at the base of the glacier play a role in accelerating retreat, as meltwater is funnelled through these channels, and is concentrated into plumes which rise across the terminus front.

2.4 Linear response of marine terminating glaciers

As noted in section 2.3, the response of all outlet glaciers draining the polar ice sheets is not totally uniform. Whilst a majority of glaciated regions are undergoing retreat and/or mass loss in response to warming atmospheric and ocean conditions, the rate, patterns, and timing of this retreat is not consistent (Radić, et al., 2014). As discussed in section 1.1, this makes the predictive modelling of climate/ice-sheet interactions very challenging. However, Cowton et al. (2018) have established a linear relationship between environmental forcing factors and terminus retreat at tidewater glaciers in east Greenland. Their study examined the relationship between annual variations in terminus positions of tidewater glaciers and annual variations of environmental forcing factors. These include surface runoff, deep ocean temperature in front of the respective fjords, and two parameterisations for combined variables which they termed M_1 and M_2. The equations describing these terms are:

$$M_1 = Q(T_O - T_f) \quad \text{Equation 1}$$

$$M_2 = Q^{1/3}(T_O - T_f) \quad \text{Equation 2}$$

where Q = meltwater runoff, T_O = deep ocean temperature, and T_f = in situ freezing point. Using these simplified environmental terms, Cowton et al. (2018) were able to explain 54% of all terminus variation across ten selected glaciers in east Greenland, and up to 76% of variability at individual glaciers. Building on this work, Fahrner et al. (2021), conducted a similar study expanded to cover all four quadrants of the GrIS. Their results implied that when averaged regionally and over multidecadal timescales, tidewater glacier terminus position anomalies changed linearly, and the effect of localised ice dynamics and geometry became insignificant in the context of the glaciers' linear responses to environmental forcing factors. A linear relationship has also been established by Slater et al. (2019) between terminus position and submarine melting, which is similarly parameterised using a combination of melt discharge and oceanic temperature variables. Comparably to Fahrner et al.'s study, this relationship was also found to be more significant when assessing a population of glaciers, rather than testing at individual sites on short timescales.

However, these results have not been consistently replicated by all studies seeking linear relationships. In a study of over 200 Greenlandic glaciers of variable fjord environments and geometries, Wood et al. (2021) found that undercutting of glaciers and ice shelves resultant from warming ocean temperatures is initiating positive feedback system through which thinning, acceleration of upstream ice, and further enhanced mass loss. They suggest that this feedback system is generating a highly non-linear response at glaciers both with and without ice shelf components, in disagreement with the studies outlined above. Establishing the applicability and reliability of linear forcing frameworks in parameterising terminus retreat is therefore an ongoing debate of great importance within contemporary glaciology.

2.5 North Greenland ice shelves

North Greenland ice shelves have been a specific focus of ice dynamical research in 2021, with the publication of several studies employing recently acquired data from

the Oceans Melting Greenland (OMG) project. The OMG project collected CTD, airborne radar ice altimetry measurements, and detailed bathymetric data during a five-year field campaign from 2016, with the primary aim of assessing the ocean-induced forcing of Greenland's glaciers, specifically through the intrusion of warm AW (Fenty, et al., 2016). Studies have included case study assessments of individual glaciers such as Humboldt (Rignot, et al., 2021), from which ocean-forcing induced undercutting has led to a tripling of mass discharge since the 1970s, as well as continent-wide assessments of AW intrusion into fjords, establishing that 49% of mass loss from the GrIS is controlled by AW undercutting (Wood, et al., 2021). However, work by Hill, et al. (2018a) has found many Greenlandic outlets with ice shelves have not yet responded strongly to this loss of mass from ice shelves, but suggest that once their shelves are lost completely and the glaciers become completely grounded, their output has the potential to increase very rapidly.

2.5.1 Petermann Gletsjer:

Petermann Gletsjer is the second largest, and most westerly of glaciers selected in this study. It is located at 80.8533°N, 60.05°W, with a catchment area of 73,927 km^2, or ~4% of the total area of the GrIS (Rignot & Kanagaratnam, 2006; Rignot, et al., 2001). Its dynamic response to a 2010 calving event in which it lost 25% of its ice shelf area (Nick, et al., 2012) has been the subject of particular interest in recent years, as researchers aim to improve models of future dynamic mass losses in response to de-buttressing. Notably, Hill, et al. (2018b) found that the velocity response of the glacier has been supressed compared with expectations following a significant mass loss, as the mass which was lost from the front of the shelf had little structural integrity as a result of extensive thinning and softening. They hypothesise that this limited response will not persist as mass is lost from stronger upstream sections in future calving events. The ice shelf discharges around 6 Gt of mass per year, and between 2007 and 2010, was found to have thinned at a rate of more than 5 m a^{-1} (Münchow, et al., 2014).

Supraglacial lakes form on the ice shelf during the summer months but may not remain on the shelf for sufficient time to destabilise the ice shelf, either due to the efficient transport of water across the shelf, or to the underlying fjord waters via rapid hydrofracture (Macdonald, et al., 2018). Washam et al. (2019) establish a strong seasonality in the basal melt rates at Petermann Gletsjer's ice shelf, inferring a correlation between increasing atmospheric temperatures in the summer months, and ocean-induced thinning. They attribute this to summer runoff enhancing fjord circulation, thus directing warmer water to the underside of the ice shelf through entrainment in the resultant plume.

2.5.2 Ryder Gletsjer:

Ryder Gletsjer is located at 81.55°N, 50.25°W. The smallest of the study glaciers, it is 29,832 km^2 in catchment area, draining 1.7% of the GrIS (Rignot & Kanagaratnam, 2006; Rignot, et al., 2001). Recently acquired bathymetric and oceanic data shows the fjord within which Ryder Gletsjer lies to have a prominent sill, which blocks warm AW from reaching the sub-ice shelf cavity (Jakobsson, et al., 2020). In comparison to Petermann Gletsjer, relatively few major investigations have been undertaken at Ryder Gletsjer. However, a detailed study by Holmes, et al. (2021) revealed a saw-tooth pattern of sudden calving and slow re-advance at the glacier's terminus and postulated that this previously stable calving cycle may be subject to change in the near future in response to velocity increases, and a gradually weakening northern front.

2.5.3 Hagen Brae:

The cumulative catchment area of Hagen Brae and its neighbouring Academy Gletsjer is 32,386 km^2, draining 1.9% of the GrIS (Rignot & Kanagaratnam, 2006; Rignot, et al., 2001). The glacier is located at 81.45°N, 27.35°W. It was recently characterised as a surge-type glacier, undergoing an increase in velocity of over 2 m per day during a

surge from 2002 to 2007. It is thought that the surge was triggered by positive feedbacks by which a build-up of englacial meltwater leads to an increase of water pressure, which eventually reached a threshold value and caused a sustained increase in velocity (Solgaard, et al., 2020). Following the surge, the glacier is now thought to be adjusting to the loss of large portions of its grounding tongue before entering either a phase of quiescence or surge.

2.5.4 Nioghalvfjerdsbræ:

Nioghalvfjerdsbræ, located at 79˚N, 25˚W, is the largest of the study glaciers, with a catchment area of 103,314 km^2, and draining over 6% of the GrIS (Rignot & Kanagaratnam, 2006; Rignot, et al., 2001). Together with its neighbouring glacier, Zachariae Isstrøm, it is forecast to contribute the majority of North Greenland's 10.9 mm addition to global mean sea level rise before 2100 (Choi, et al., 2021). Nioghalvfjerdsbræ holds ice volume with an equivalent potential sea level contribution of 0.54 m and has lost between 53 and 99 m a^{-1} of grounded ice since 1979 as a response to ocean forcing (An, et al., 2021). Its bathymetric configuration if thought to be relatively stable, especially in comparison to Zachariae Isstrøm, as AW intrusion to the subglacial cavity is limited by a sill which sits at the entrance to the fjord, blocking entrance of deep AW (An, et al., 2021).

2.6 North Greenland Climate

The East and West coasts of Greenland are flanked by major oceanic currents including the West Greenland Current and Norwegian Atlantic Current, illustrated in Figure 3 from Catania et al. (2020). The North coast is dominated to a lesser extent by these strong circulation systems, being protected somewhat by the narrow, and shallow Nares Strait, and subject instead to much weaker, northerly currents originating from the Eurasian basin (Timmermans & Marshall, 2020). Hagen Brae and Nioghalvfjerdsbræ are particularly influenced by these northerly currents including

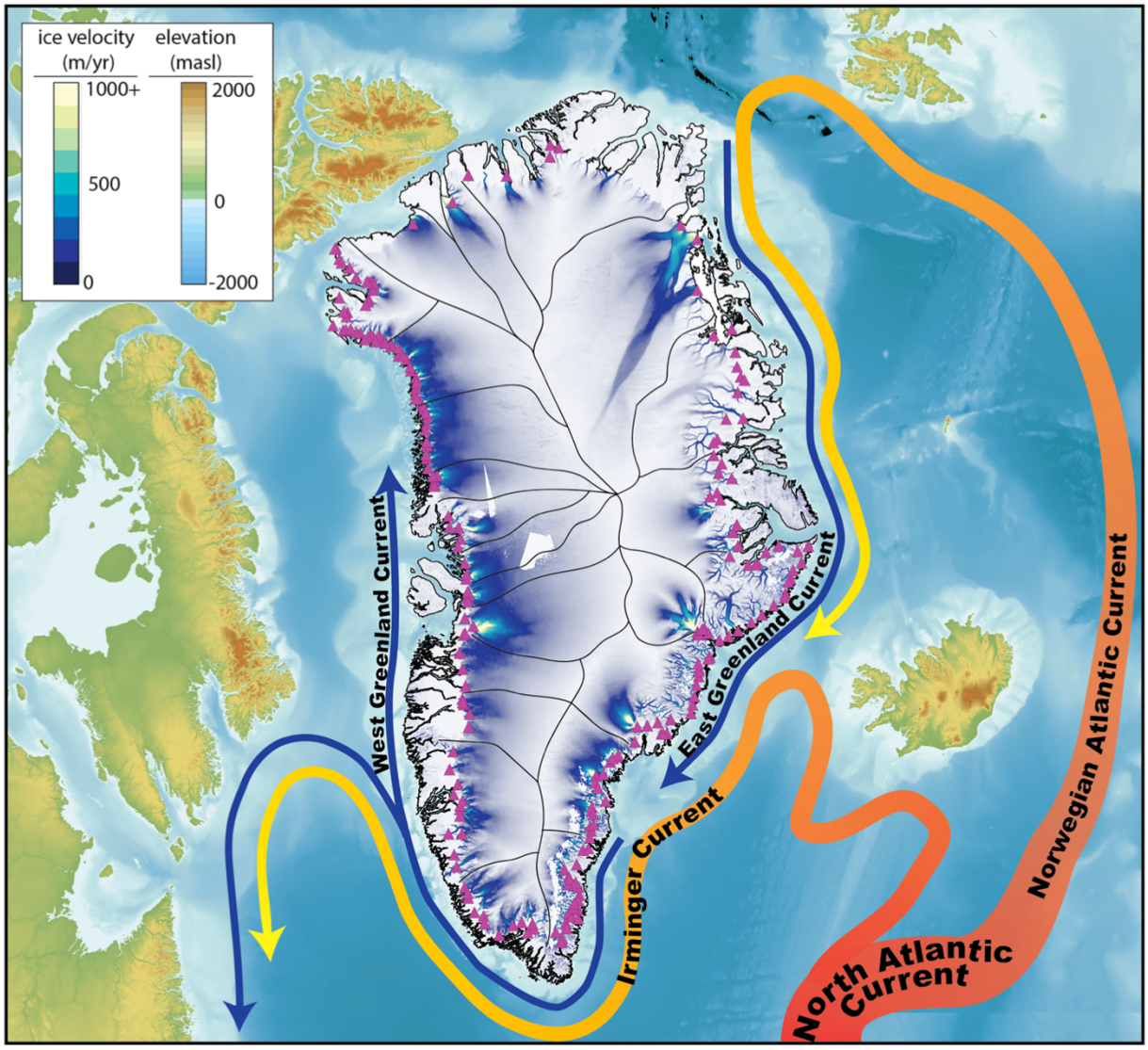

Figure 3: *Arctic Ocean currents surrounding Greenland, from Catania, et al. (2020). The map shows surface ice velocity, with the fastest flowing (> 50m a^{-1}) indicated by triangles. Bathymetry data shows troughs extending from ice sheet to edge of continental shelf, and ocean current size and heat transport are indicted by the size and colour of arrow respectively.*

the East Greenland current, as they are located on the more exposed Easterly coast. Circulation in the Nares Strait is westward, channelling cold, fresh Polar Water into the Labrador Sea (Shroyer, et al., 2015). However, fjord waters across North Greenland have largely comparable properties to many of those around the continent. Specifically, the waters increase in temperature with depth, as warm, salty AW circulates below the fresh Polar Water, leading to a stratification in both the ocean

waters surrounding the fjords, and subsequently the fjord waters bathing the glaciers (Straneo, et al., 2012). The general pattern of change to ocean temperatures in the waters surrounding Greenland from the early 1990s to ~2017 has been one of warming in three key phases (Wood, et al., 2021). From 1992-1997, ocean temperatures across North Greenland were relatively stable, with a rapid warming of around 0.19˚C per year beginning in 1998. This warming period lasted for nine years, before a shift to a slow cooling phase at around 0.11˚C per year began in 2008 and has remained in this phase until 2017. However, these trends are not uniform, with the north-easterly regions experiencing much less cooling from 2008 onwards than the central north and north-westerly regions.

Atmospheric temperatures along the coasts of Greenland have warmed by 1.7 ˚C during summer months and more than 4˚C during winter months since the early 1990s (Hanna, et al., 2021); these values are greater than the global average by nearly double, as a result of arctic amplification (Cohen, et al., 2020). North Greenland is particularly vulnerable to this warming, with its ablation zone expanding at twice the rate of the southern regions in response to shifting atmospheric circulation patterns reducing summer cloud cover, and consequently albedo in the North (Noël, et al., 2019). Long-term, near-surface air temperature measurements are collected from just 18 sparsely distributed weather stations across the surface of the ice sheet (Steffen, et al., 1996), and so several investigations have used isotopic data from ice cores to improve constrains of regional temperatures since the early 1990s. With these studies has come a resultant improvement to the climate models used to interpolate air temperature, and subsequently runoff (Orsi, et al., 2017). The North Greenland Eemian Ice Drilling Project has been particularly useful, and work on isotopic data collected from gas bubbles in this core suggests a regional North Greenlandic warming of 2.3-3.0 ˚C from the early 1990-1970 mean (Orsi, et al., 2017). Shallow cores from across the North Greenland interior have found a comparable increase of 0.9-2.5 ˚C per decade over the 50 years from 1966 (Kjær, et al., 2021).

It should be noted that this increase in temperature has not been uniform each decade. The North Atlantic Oscillation (NAO) has played a role in governing inter-annual air temperature variation, most notably when a rapid shift from negative to positive NAO conditions in 2013 resulted in a sudden decline in mass loss from the GrIS (Bevis, et al., 2019).

2.7 Remote sensing of ice shelves

Whilst measurements of the calving front are straightforward to obtain in the satellite era because of extensive and rapidly improving 30 m resolution satellite imagery, studies measuring changes to ice shelves over time are hindered by very low availability of in situ grounding line measurements. To obtain these measurements directly requires detailed and expensive field campaigns, and the most economically viable method to measure grounding line positions is therefore through remote sensing. This includes methods such as assessing the change in slope from upstream ice grounded on steep topography to flat ice shelves at hydrostatic equilibrium using altimetry data (such as that from the ICESat and CryoSat-2 missions) (Dawson & Bamber, 2017). Whilst this method has been employed in several ice shelves around Antarctica, its limited accuracy of around 1 km cannot be considered appropriate for application to Greenlandic glaciers where changes to grounding line position within smaller fjords may be less than this value over several years. Differential interferometry (description of method given in section 3.1.2) is considered the more accurate and appropriate methodology in almost all circumstances (Friedl, et al., 2020) but requires extensive and specialised processing of SAR data to obtain measurements.

3. Methods

3.1. Data acquisition

3.1.1 Satellite imagery

Natural colour imagery used to digitise calving front position was obtained from the Landsat-5, -7 and -8 satellites. Synthetic aperture radar data from Sentinel-1 was excluded from this study because of the respective under- and over-estimations of calving front position which resultant images acquire during descending or ascending orbits (Lea, 2018). When combined with the optical satellite imagery required to obtain a record of positional change over the entire study period, this would lead to inconsistencies in the error associated with each terminus position measurement. Sentinel-1 data is also subject to inaccuracies in regions where substantive thinning or other deviation from the DEM used to constrain the image's geolocation may have

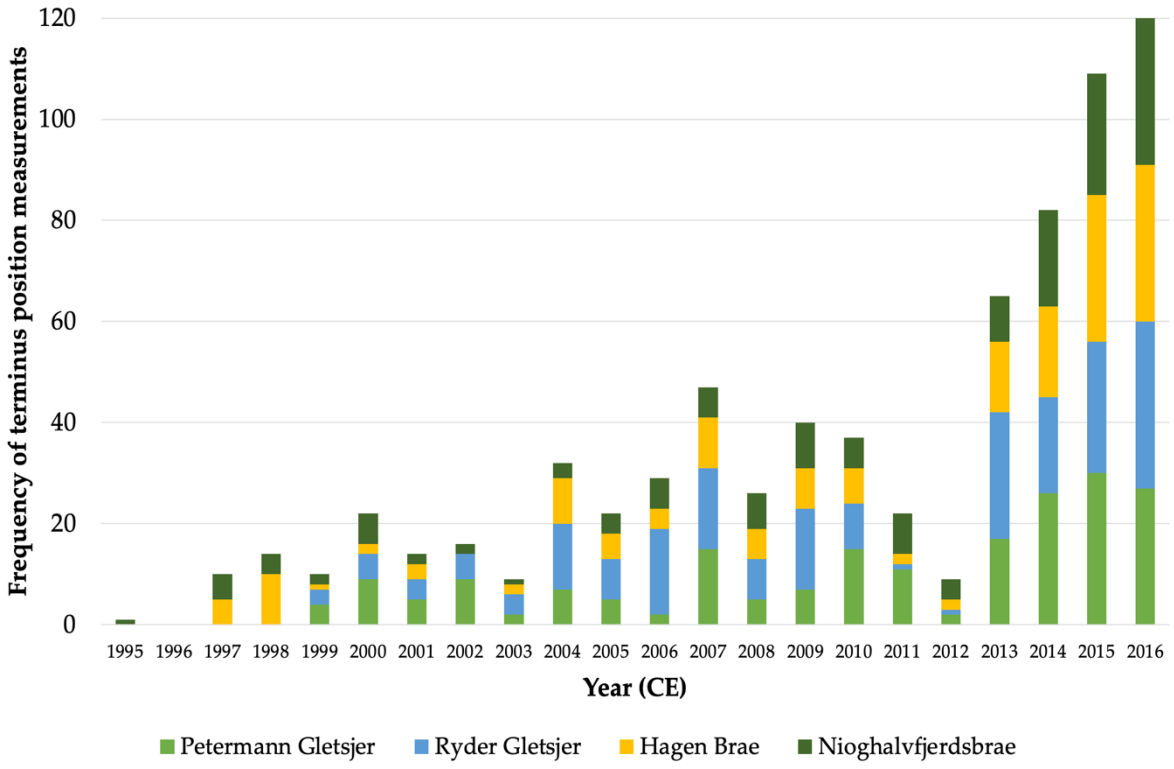

***Figure 4**: Frequency distribution of terminus position measurements over the study period.*

occurred (Nagler, et al., 2015), and so is not considered suitable for application in this study's assessment of highly dynamic ice shelf environments.

Data availability from the Landsat project is inconsistent across the study period, with only very limited examples of data from the Landsat-5 mission matching the specified criteria for terminus digitisation (detailed in section 3.2.1). A resultant step-change in data availability occurs following the launch of Landsat-7 in 1999, and again in 2013 with the launch of Landsat-8. There are therefore several years in the early study period where no suitable satellite images are available. Consequently, the measurements of Ryder Gletsjer and Petermann Gletsjer are taken only from 1999 onwards, and measurements to Hagen Brae begin in 1997, rather than the years in which the first grounding line position was obtained (1995/6). Suitable images were available dating back to 1995 at Nioghalvfjerdsbræ, but a gap in the data exists due to no suitable images being available in 1996. A second data gap occurred at Hagen Brae, where no suitable images were available for terminus measurement in 2002. Figure 4 summarises the distribution of terminus measurements across the study period.

3.1.2 Grounding line positions

Grounding line positions were obtained from the European Space Agency's (ESA) Climate Change Initiative (CCI) program. The ESA obtained grounding line positions at the four study sites using synthetic aperture radar (SAR) data. 1995/6 grounding line positions were obtained from ERS-1/2 TANDEM satellite mission, whilst 2017 positions were obtained from the SAR sensor onboard Sentinel-1 (Nagler, et al., 2018). The grounding line positions were identified using differential interferometry of SAR images (DInSAR). DInSAR is a technique through which vertical displacement of the Earth's surface is measured using two SAR images covering the same location. This is a useful measurement in differentiating ice shelves from grounded ice, as the floating component will shift vertically with the tides each day to maintain hydrostatic equilibrium with variable local tidal heights, whilst the grounded ice experiences

negligible vertical deflection over the same period (Fricker & Padman, 2002). Phase information corresponding to each image are differenced from one another to create an image which displays phase-shift between the two images. This correlates to the displacement of the measured surface over the time between image acquisitions (Goldstein, et al., 1993). Through removal of the horizontal displacement component by differencing two pairs of images acquired at different tidal conditions within a period of a few days to maintain coherence, a plot is produced which details degree of vertical ice flexure. The plot uses colour-coded symbology corresponding to magnitude of displacement; the more closely spaced the fringes of colour, the greater the degree of vertical displacement between the two pairs of SAR images (Yamanokuchi, et al., 2005). The 2015 DInSAR image used to measure grounding line position by the ESA at Petermann Gletsjer is shown in Figure 5, with annotations showing the subsequently derived limits of seaward and landward ice flexure on

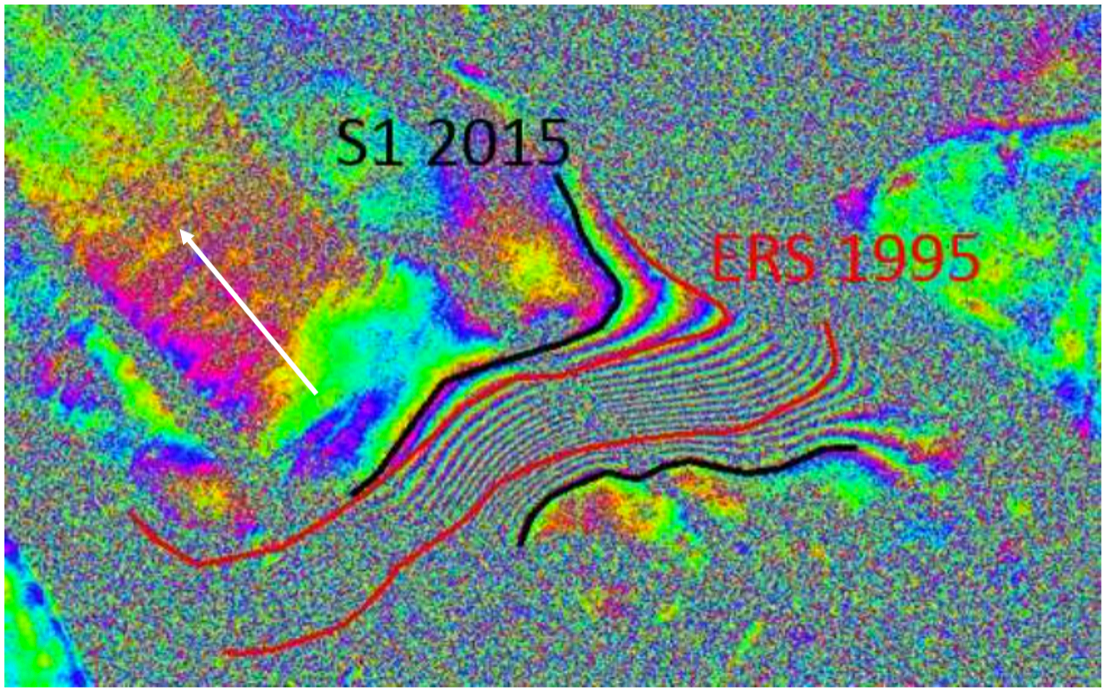

***Figure 5**: From Nagler, et al., 2018. Double difference interferogram of Petermann Gletsjer's grounding zone acquired from Sentinel-1 SAR imagery in 2015. The characteristic close spacing of colored fringes in the centre of the image denotes the region of ice subject to tidally induced vertical flexure. The inward and seaward limits of this zone are noted both for the 2015 measurements (black lines) and 1995 measurements (red lines). Direction of ice flow marked by white arrow.*

.

either side of the tidal deformation zone, visible as a tightly spaced section of fringe pattern. The standard error of DInSAR for measuring inward limits of ice flexure as measured by Rignot et al., (2011) is ± 100 m.

Raw products available from the ESA measured both the landward and seaward limits of tidal flexure, but for the purpose of this analysis, the landward limit was isolated as the more suitable proxy for grounding line position following the framework of grounding zone anatomy established by authors including Vaughan (1994), Fricker and Padman (2006), and Dawson and Bamber (2017). It should be noted that the landward limit of flexure is likely to have some ingrained seaward bias from the true grounding line position, as every interferometric sampling technique is limited by the sensitivity of its vertical displacement measurements (Friedl, et al., 2020). Direct measurement of grounding lines using break-in-slope mapping (Hogg, et al., 2018) was considered during the formulation of this project but would have been severely limited by low temporal resolution and coverage of DEM availability over the study area. Thus, the more accurate technique of using secondary DInSAR data was considered more suitable for this application.

3.1.3. Oceanographic reanalysis data

Ocean temperature reanalysis data was obtained from the Copernicus Marine Environment Monitoring Service (CMEMS), who produce a multi-model ensemble (GREP-V1) detailing daily and monthly 3-dimensional estimations of global ocean temperature, as well as other variables such as salinity and sea surface height. The ensemble represents the mean of four different model outputs: ECMWF's ORAS5 model (Zuo, et al., 2019), Mercator Ocean's GLORYS2V4 model (Lellouche, et al., 2013), GloSea5 from the UK Met Office (MacLachlan, et al., 2015), and C-GLORS05 from CMCC (Storto, et al., 2016). ORAS5, C-GLORS05, and GLORYS2V4 use slightly different iterations of the NEMO ocean model coupled with the LIM2 sea-ice model to estimate historical ocean conditions, whereas GloSea5 couples NEMO with the

CICE4.1 sea ice model. The hindcasts are constrained with a variety of observational data, including EN4 in-situ profiles of ocean water column temperature and salinity (Good, et al., 2013), Reynolds SST (Reynolds, et al., 2002), HadlSSTv2 SST (Titchner & Rayner, 2014), and CORA (Cabanes, et al., 2013).

The most significant sources of variation between the models are the parameters of their surface forcing components. For example, GLORYS2V4 is the only model which does not include sea surface temperature and salinity nudging but does includes climatological runoff and ice shelf melting as model components. ORAS5 is the only model to include surface waves forcing in its analysis, and C-GLORS05 also incorporates sea ice concentration surface nudging. There are also variations in the methodology each modelling group uses to assimilate the data with their chosen observational measurement, with assimilation windows ranging between a 1- and 4-days. Each of these models has benefits and drawbacks associated with them, and so an ensemble product was chosen over any single model as it reduces the significance of major anomalies in any one product. It also increases the total amount of observational data included in the reanalysis as no individual model makes use of all available datasets. Resultantly, the GREP-V1 ensemble has a global root mean square (RMS) difference of less than 1°C when compared to the CORA dataset of in situ ocean temperature observations (Desportes, et al., 2019). It should be noted that RMS error decreases significantly across all depth levels following the onset of data collection from the ARGO ocean observation programme in 2002 (Roemmich, et al., 2009).

The CMEMS product specifies mean monthly ocean temperature from these models in 75 depth layers, across which the height of each layer increases incrementally from the surface (which has a layer height of ~1 m) towards the lowest available depth of 5902 m below the surface (layer height of ~ 100 m). Its resolution is 1/4°, corresponding to approximately 9 km x 9 km pixels in the Arctic, which is less than half the width of the narrowest point of the Nares Strait (~ 25 km). Crucially, this means that data is available in the ocean water adjacent to the Petermann and Ryder Fjords, in addition to offshore data in the open ocean adjacent to Hagen Brae and

Nioghalvfjerdsbræ which is more widely available in lower-resolution ocean temperature reanalysis products.

3.1.4. Runoff reanalysis data

Runoff reanalysis data covering North Greenland with a resolution of 1x1 km was obtained from a version of the Regional Atmospheric Climate Model (RACMO2.3p2) (Noël, et al., 2018 and personal comm.). The data obtained for this study is an extension of Noël et al. (2019), who produced a study applying the model to show differential ablation zone expansion rates across Greenland. The RACMO2.3p2 model is described fully by Noël et al. (2018). Most notably, it is tailored to replicate the climatic conditions of the GrIS and can simulate a variety of complex snowmelt, water retention and mass transfer processes across the surface of the ice sheet. The model is constrained by observational data from automated weather stations (AWSs) across the ice sheet, although it should be noted that the concentration of AWSs is sparse along the North Greenland coast compared to the more accessible West Greenland coast. The model therefore also considers in situ measurements of surface mass balance (SMB) and annual glacier discharge at Nioghalvfjerdsbræ (Mouginot, et al., 2015), in addition to SMB measurements from the ablation zone of Petermann Gletsjer (Machguth, et al., 2016).

Runoff is a product of many variables within the model, each of which has a quantifiable amount of error associated with it when compared to observational data (detailed fully in Noël, et al., 2018). The variable model outputs correlate well with observed data ($R^2 \geq 0.92$), with the exception of shortwave upward and longwave downward radiation ($R^2 = 0.88$ and 0.83 respectively), and wind speed ($R^2 = 0.68$). Though the accuracy of runoff specifically is not quantified by the modelling group, the high degree of correlation demonstrated by its constituent components in the model implies a high degree of confidence in its reliability.

3.1.5 Subglacial bed topography and fjord bathymetry

Data from the BedMachine v3 project (Morlighem, et al., 2017) was also downloaded to extract information about subglacial topography, fjord bathymetry, and topographic profiles of the grounding lines. It was also used to delineate catchment areas in order to extract runoff data (section 3.2.4).

3.2 Measurement and Analysis

3.2.1 Calving front digitisation

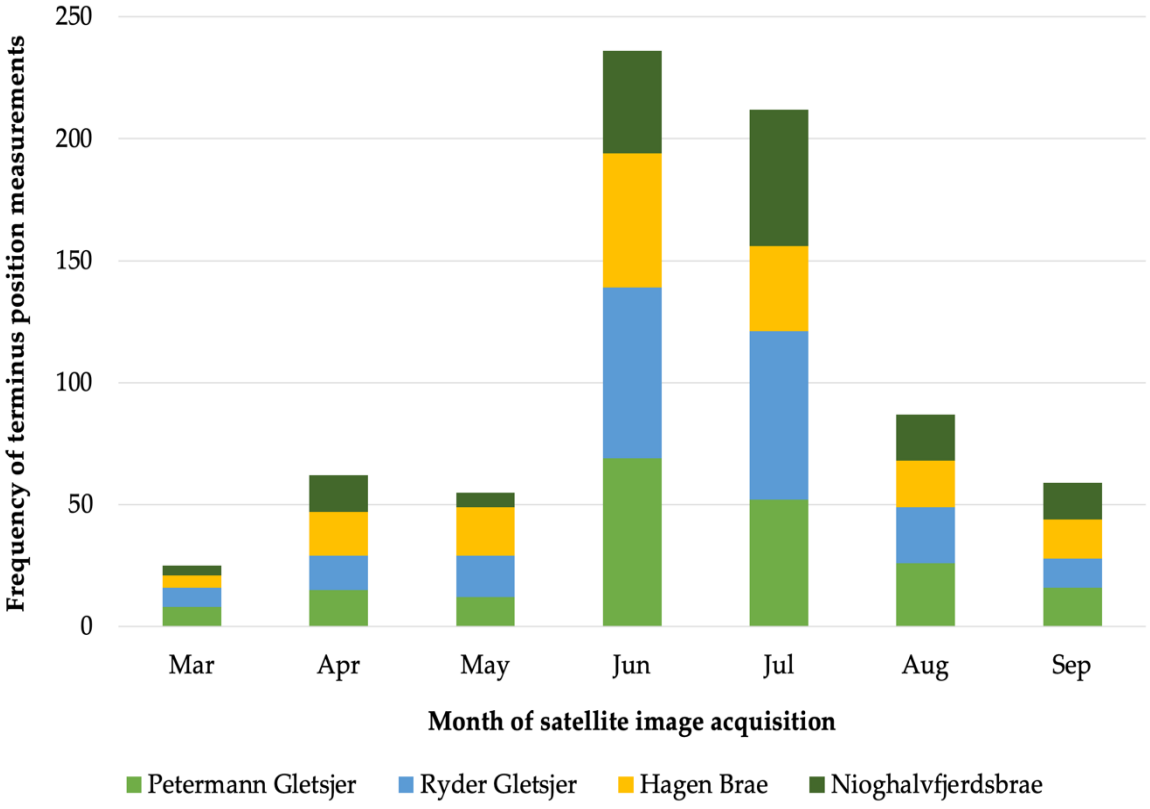

***Figure 6**: Frequency distribution of terminus position measurement month of acquisition over the study period.*

The calving fronts of the five glaciers were digitised in Google Earth Engine (GEE), using GEEDiT (GEE Digitisation Tool), developed by Lea (2018). The tool makes use of GEE's extensive cloud-based library of satellite imagery including all Landsat and Sentinel mission data, to negate the time-consuming task of identifying, downloading,

and subsequently uploading suitable satellite imagery into GIS software. Instead, users can filter imagery intersecting a specified location using criteria including cloud cover, satellite, and study period, and visualise all images matching these criteria in sequence according to the date of acquisition. The tool also enables users to manually generate polylines for export to shapefiles denoting ice margin positions on a continuous basis whilst browsing satellite data.

During digitisation Landsat images were visualised in GEEDiT using a natural (RGB 3-2-1) band combination, and Landsat-7 and -8 images were pansharpened to improve the resolution of multi-spectral imagery. In order to minimise the impacts of seasonal terminus position oscillation whilst also allowing for maximum data collection in data-sparse years, satellite images acquired between 1st March and 31st September were used, although 73% of images used for digitisation were acquired in June, July, or August. The distribution of image sampling across these months over the study period is shown in Figure 6. Only images which had completely unobscured views of the terminus were considered appropriate for digitisation, to minimise error caused by cloud or extensive shadow obscuring margin details. In several years, portions of the calving front of Petermann Gletsjer and Nioghalvfjerdsbræ were tightly packed by dense and continuous ice mélange. This mélange was included in measurement of the terminus position, as these features tended to remain in position throughout annual summer seasons and thus were considered to form a rigid, constituent part of the ice shelf (Sakakibara & Sugiyama, 2019). In total, 744 frontal positions were digitised.

Potential error associated with calving front digitisation can result from both inaccuracies in the manual digitisation of margins, and the limited resolution of satellite imagery. Commonly, digitisation following the methodology outlined above is limited primarily by the latter, as error associated with manual digitisation does not generally exceed the resolution of satellite imagery in the public domain (DeBeer & Sharp, 2007; Carr, et al., 2013; Moon, 2014). For confirmation, measurement inaccuracy was quantified through repeat digitisation of a single image per satellite at Ryder

Gletsjer (n = 10). The mean error of these digitisations compared to the original measurement used in this study was 20.21 m for Landsat-5, 17.61 m for Landsat-7, and 9.85 m for Landsat-8, with a subsequent overall digitising error of 15.9 m. Each of the Landsat satellites has a 30 m resolution in its blue, red, and green bands, and so a measurement of change between any two points may have a maximum associated error of ±60 m.

The multi-centreline method of measuring terminus change was chosen for this study as it enables the visualisation of spatial variability in calving front motion, which none of the more traditional methods (e.g. box method, bow method) allow for (Lea, et al., 2014; Lea, 2018). Nine centrelines per glacier were digitised using GEEDiT Reviewer (Lea, 2018), the most central of which at each study site is shown in Figure 7. Changes to terminus position were undertaken using MaQiT, a complementary MATLAB script developed for use in conjunction with GEEDiT (Lea, 2018), which computes changes in terminus position along specified centrelines.

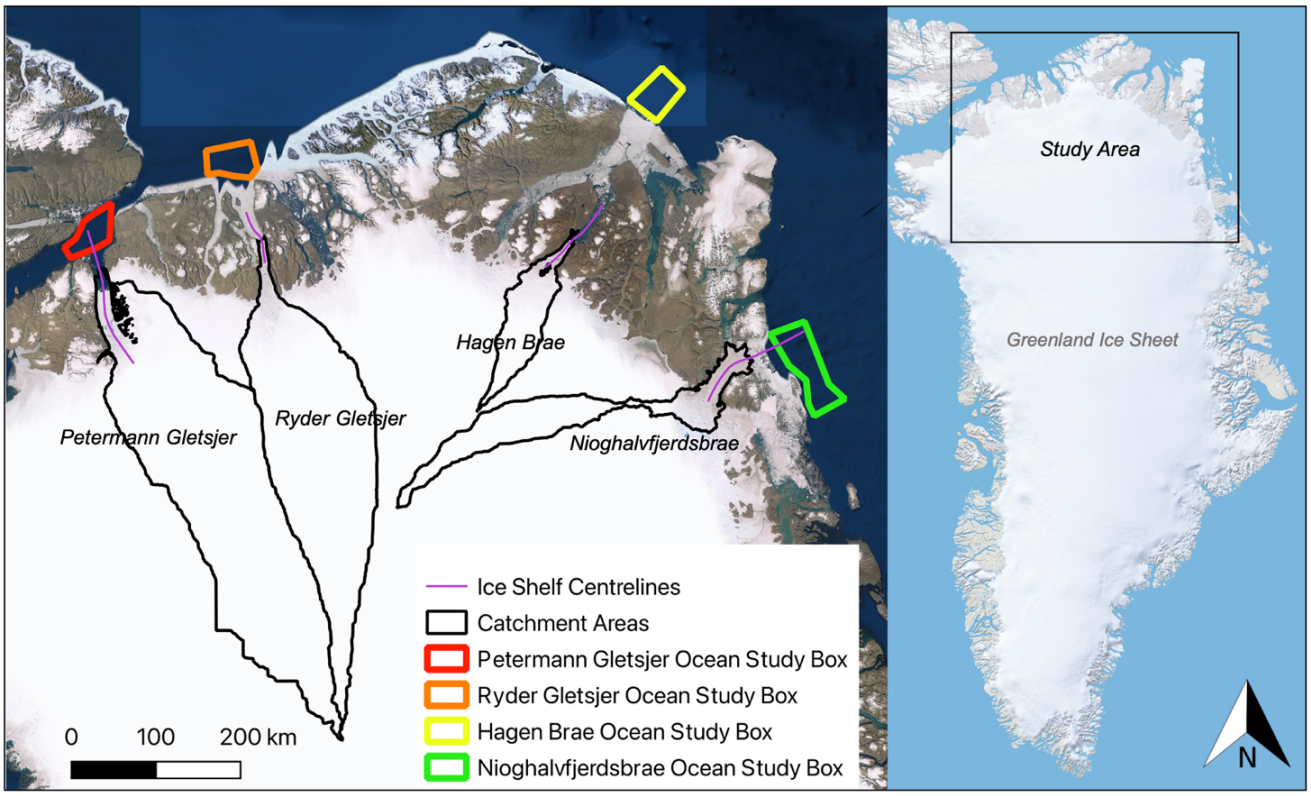

***Figure 7**: Map of study areas across North Greenland showing centrelines over which terminus change was measured, superimposed over delineated catchment areas, and ocean sample boxes. Background imagery from ESRI.*

3.2.2 Grounding line interpolation

Annual grounding line position was interpolated between the CCI measurements in 1995/6 and 2017 through a sequence of geoprocessing operations in ArcGIS and QGIS. Firstly, a framework along which to measure change was constructed through the digitisation of polylines between vertices of each InSAR-derived shapefile. The polylines were positioned to maintain the shape of the end-member grounding lines during interpolation. Using the QChainage plugin, nodes were generated dividing the polylines into a specified number of equal segments (n = length of study period in years) to determine annual grounding line position based on the average rate of change between InSAR measurements. The nodes were assigned attributes based on their representative year, split from their existing files and re-merged into separate groups according to year. They were then converted from point to line data using a sorting system based on the node's position relative to the most easterly valley wall. Average migration rate was also quantified between the two InSAR measurements along multiple centrelines per glacier using MaQiT. It must be noted that interpolation is not equivalent to direct measurement. However, direct measurement of grounding lines through interferometry was not feasible within the scope of this study due to the intense computational training necessary to undertake work with this data. Interpolation is therefore considered necessary to provide a mechanism by which the magnitude and direction of grounding line change can be used to constrain changes to ice shelf area.

3.2.3 Ice shelf area quantification

The area of each glacier's ice shelf in each year of the study period was measured by merging each year's calving-front and grounding-line positions with an additional polyline delineating the fjord walls of each glacier and applying the QGIS Polygonise tool on the resultant multiline vector. Each year's sampled terminus position was chosen to be the measurement taken closest to 1st July, to minimise the effect of

seasonal variability skewing results. A summary of the measurements made at each glacier to calculate ice shelf area is shown in Table 1.

	Petermann Gletsjer	***Ryder Gletsjer***	***Hagen Brae***	***Nioghalvfjerdsbræ***
Earliest InSAR GL position	1995/10/28	1996/03/27	1996/03/16	1995/08/28
Latest InSAR GL position	2017/02/11	2017/01/06	2017/03/16	2017/03/05
Earliest margin digitisation	1999/07/09	1999-07-18	1997-05-02	1995-09-08
Latest margin digitisation	2016-09-28	2016-09-13	2016-09-23	2016-09-26
Location (from Bjørk, et al., 2015)	80.8533°N, 60.05°W	81.55°N, 50.25°W	81.45°N, 27.35°W	79°N, 25°W
Calving front positions digitised (n)	198	213	176	157

***Table 1**: Summary of measurements made at each glacier*

3.2.4 Runoff analysis

Drainage basins of the GrIS were delineated using a suite of hydrological analysis tools available through ArcGIS and QGIS. These drainage basins are shown in Figure 7. DEM inputs for this analysis were sourced from the BedMachine v3 project (Morlighem, et al., 2017). For the purposes of this analysis, individual catchment areas which drained onto the ice shelves were merged to ensure that all runoff making its

way to the fjords via ice shelves – and therefore contributing to meltwater plumes – is accounted for, although it should be noted that some of these glaciers have individual classifications and are not considered to be constituent parts of the study glaciers according to Bjørk et al. (2015). Namely, the catchments of Porsild Gletsjer, Sigurd Berg Gletsjer, Hubert Gletsjer, and Belgrave Gletsjer have been included as they drain directly onto the Petermann Ice Shelf. In this study, the area of Petermann Gletsjer's runoff catchment is calculated to be 62,573 km^2, Hagen Brae to be 7,378 km^2, Ryder Gletsjer to be 43,469 km^2, and Nioghalvfjerdsbræ as 14,202 km^2. These catchment areas differ substantially from previously delineated glacier areas (Rignot & Kanagaratnam, 2006) as glacial catchment area is typically measured using a combination of velocity measurements and bed topography maps to route the flow of ice over the bed, rather than water over the ice surface e.g. (Lewis & Smith, 2009). Having defined catchment areas, annual cumulative runoff data was clipped to the size and location of each of the four basins, and subsequently the annual sum of runoff across all pixels of the catchment each year was measured.

3.2.5 Oceanographic analysis

Monthly ensemble-mean ocean temperature data surrounding North Greenland was packaged into annual files over the study period 1995-2016 and downloaded from CMEMS in 4-dimensional NetCDF format (Gounou, et al., 2020). The data was masked to cover each study area in turn using predefined sample boxes ranging from 1841 km^2 in the waters in front of Petermann Gletsjer's terminus to 3646 km^2 in front of Nioghalvfjerdsbræ (all study boxes shown in Figure 7). The variation in study size is due to constrains on sampling imposed by local topography and bathymetry: to take a useful sample of ocean temperature, waters of a comparable depth to the depth of the grounding line of each glacier are required. The waters sampled should also be outside the entrance to fjords, as the accuracy of circulation models improves with distance from these complex environments, which are not well resolved by global

ocean circulation models. The measurements also needed to remain within the limits of the continental shelf. The sample box associated with Petermann Gletsjer is constrained in size by the width of the Nares Strait. The oceanographic sample boxes in front of Ryder Gletsjer and Hagen Brae were drawn to be of a comparable size to the Petermann sample (within ~150 km^2), whilst the Nioghalvfjerdsbræ sample box is nearly twice as large, due to the very shallow waters in front of the fjord entrance necessitating an expansion of the box to sample deeper waters to the northwest and southeast of the fjord entrance. Key statistics associated with each study box are detailed in Table 2.

Mean surface-water temperature (0-200 m.b.s.l.) and deep-water temperatures (200-800 m.b.s.l.) were derived from the masked oceanic data. A maximum depth of 800 m below sea level was chosen to correspond with the deepest point which a grounding

	Petermann Gletsjer	**Ryder Gletsjer**	**Hagen Brae**	**Nioghalvfjerdsbræ**
Mean depth below sea level within study box (m)	-546	-590	-172	-288
Maximum depth below sea level within study box (m)	-859	-767	-765	-579
Minimum depth below sea level within study box (m)	169	-412	-109	-3
Area of sample box (km^2)	1841	1953	1981	3646

Table 2: *Statistics associated with the depth range of each sample box. The Petermann sample box includes a small island which is why the minimum depth below sea level is positive.*

line reached over the study area. Annual averages of these monthly temperature values were then calculated by averaging the twelve 4th dimensional components of monthly temperature across all other dimensions using MATLAB's TMean function, as was the subsequent depth-specific annual temperature of all pixels within the study area to extract a single annual value of oceanic temperature. MATLAB code used to undertake oceanographic analysis and plot figures is fully detailed in the appendix.

3.2.6 Combined environmental forcing variables

The effect of meltwater runoff and ocean temperature are combined into parameterisations for the cumulative effect of environmental forcing factors M_1 and M_2 according to methodology devised by Cowton et al. (2018). The equations used to derive these parameterisations are detailed in section 2.4 (equations 1 and 2).

3.2.7 Statistical analysis

To ascertain whether a statistically significant relationship was present between average annual terminus position and any of the environmental forcing factors, an Engle-Granger test for cointegration between each non-stationary variable was run (Engle & Granger, 1987), because this gives consistency of testing with the approach used by Cowton et al. (2018). Simple linear regression was also examined, but it should be noted it is possible for liner regression tests to describe correlation where in fact none exists (Granger and Newbold, 1974). The time series of ice shelf area was not tested for a linear relationship with environmental forcing factors as the measurements were constrained by grounding line positions which had been linearly interpolated. Therefore, in cases where the grounding line migration played a greater role in determining areal change than terminus position, linear change to the ice shelf area may have been an artefact of the methodology used to measure change.

4. Results

4.1 Measured changes to ice shelves

4.1.1 Changes to grounding line positions

Of the four grounding study sites, only Nioghalvfjerdsbræ underwent net advance. Each of the other grounding lines retreated across their entire width between 1995/6 and 2017. At Petermann Gletsjer, the total mean grounding line retreat over the

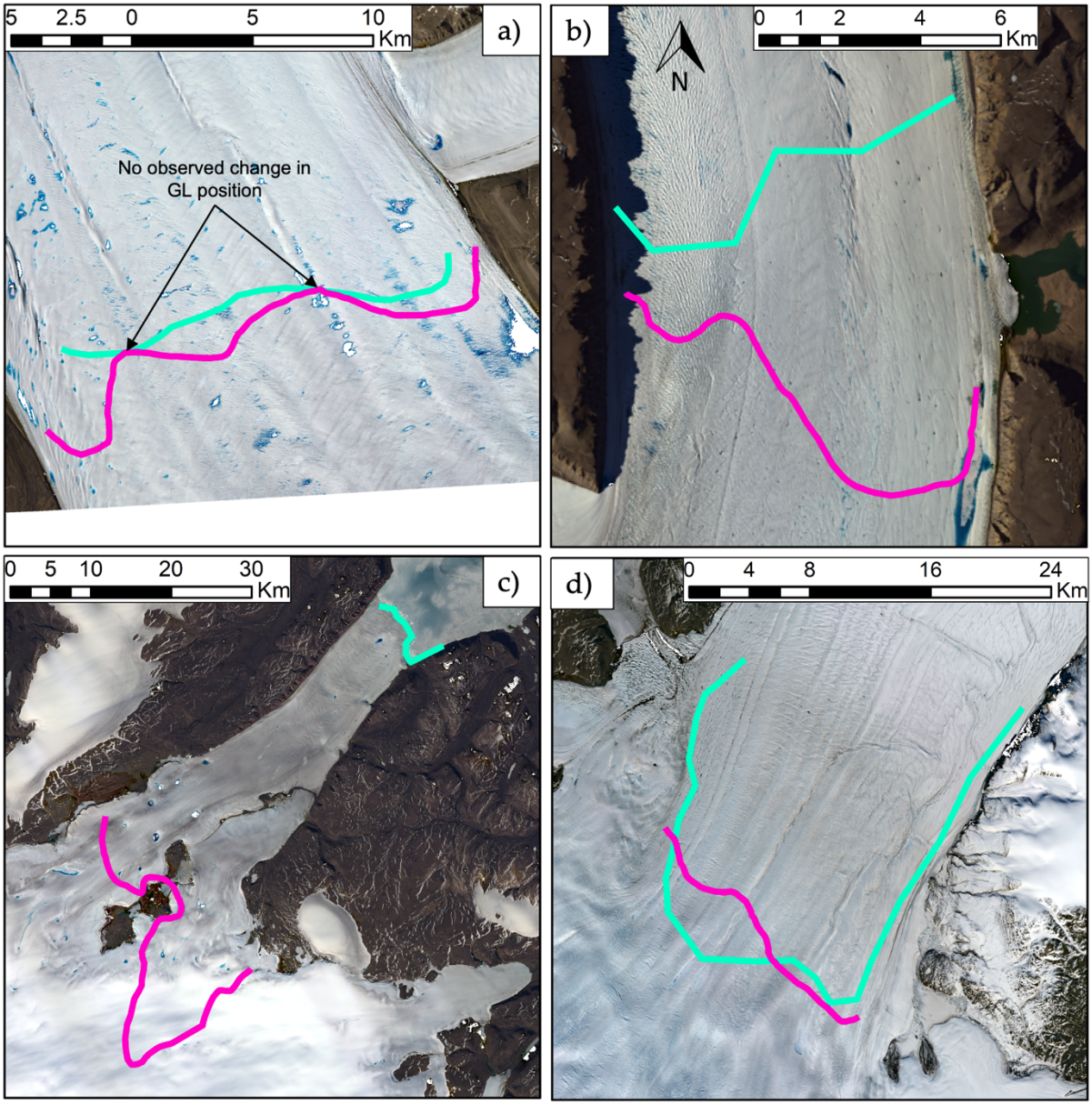

***Figure 8**: InSAR-derived grounding line position in 1995/6 (cyan) and 2017 (magenta) over Landsat 8 imagery from July 2016 at a) Petermann Gletsjer, b) Ryder Gletsjer, c) Hagen Brae, d) Nioghalvfjerdsbræ.*

calculated across multiple centrelines was 1,214 m, corresponding to a mean annual retreat rate of 55 m a^{-1}. The retreat rate across different centrelines varied slightly, ranging from between 0 and 193 m a^{-1}. The most significant retreat occurred along the western side of the fjord, with two notable portions of the grounding line in the central fjord which underwent negligible migration across the study period (annotated in fig. 8a). Ryder Gletsjer retreated by an average of 5,689 m across its width, with a resultant mean annual retreat rate of 271 m a^{-1}. Ryder's grounding line retreat was more extensive in the eastern fjord, with a maximum retreat in this zone of 9107 m across the study period. The minimum observed retreat across the grounding line was 1843 m, which occurred in the western fjord.

Hagen Brae's grounding line retreated by an order of magnitude more than Ryder Gletsjer, undergoing an average of 51,896 m of retreat across its width from 1996 to 2017. On average, this equates to a mean retreat rate of 2,471 m a^{-1}, just under half of Ryder's total grounding line change. The retreat at Hagen Brae's grounding line varies from a minimum of 44,771 m at its centre, to a maximum of 67,679 m in the more southerly section of the fjord. In contrast, Nioghalvfjerdsbræ, located just 250 km to the southeast of Hagen Brae, underwent a net advance of 701 m across its width over the study period, equating to an average annual advance of 32 m a^{-1}. However, this positional change was not uniform. Whilst the central sections of the grounding line advanced by a maximum of 4659 m over the study period, change at the margins of the grounding line was in the opposite direction. The most northerly portion of the grounding line retreated by 4934 m, and the most southerly by 1183 m.

4.1.2 Changes in bathymetry at the grounding line

As grounding lines migrate over time, the characteristics of the bathymetry on which they rest can change. At Petermann Gletsjer, the 1995 grounding line position rested at a mean depth of 504 m.b.s.l, and at its deepest, rested at 584 m.b.s.l. By 2017, it had retreated into a portion of the fjord with a shallower mean depth of 469 m.b.s.l., but

had a greater maximum depth of 616 m.b.s.l. Clearly visible in Figure 9, this is due to the retreat of the eastern portion of the glacier into a deep channel within the bed. The two regions of almost stationary grounding line migration at Petermann Gletsjer correlate directly to bathymetric highs in the fjord below (annotated in fig. 9a). Ryder Gletsjer underwent a similar pattern of retreat into deeper waters between 1996 and 2017, moving from a mean fjord depth at the grounding line of 451 to 511 m.b.s.l., and a maximum depth of 751 to 803 m.b.s.l., the deepest point of any grounding line measured throughout this study. The grounding line profile altered significantly, with a previously isolated deep eastern channel in 1995 widening to cover around 33,000 m of the grounding line by 2017 (fig.9b). At Hagen Brae, mean grounding line depth has increased with retreat from very shallow fjord waters of 125 m.b.s.l. to deeper inland waters of 234 m.b.s.l. The maximum depth also increased from 239 to 378 m.b.s.l. Hagen Brae's grounding line profile changed significantly between 1996 and 2017 from a very shallow overall profile with a prominent channel on the northern portion of the grounding line and much shallower, smaller channels on a shelf in the southern fjord, to a very steep-sided, flat-bottomed single channel (fig. 9c). It should be noted that in Figure 9c, only values below sea level are plotted as many of the BedMachine v3. values in the northern portions of the plotted grounding line are above sea level and therefore are not comparable with ocean temperature data. The grounding line of Nioghalvfjerdsbræ has advanced from deeper inland water with a mean depth of 528 m.b.s.l. to shallower bed topography with a mean depth of 522 m.b.s.l. The maximum depth also decreased between 1995 and 2017 from 625 to 587 m.b.s.l. The profile of the grounding line changed significantly from approximately even in depth across its width apart from one deep central channel to a profile showing two very distinct channel systems composing most the grounding line's width. The deepest portions of the more northerly channel correlates to the portion of the grounding line which has advanced the most, whilst the much shallower, more southerly channel correlates to retreat of the above grounding line (annotated in fig.

9d). At a notable topographic high between the channels, grounding line position has remained stable.

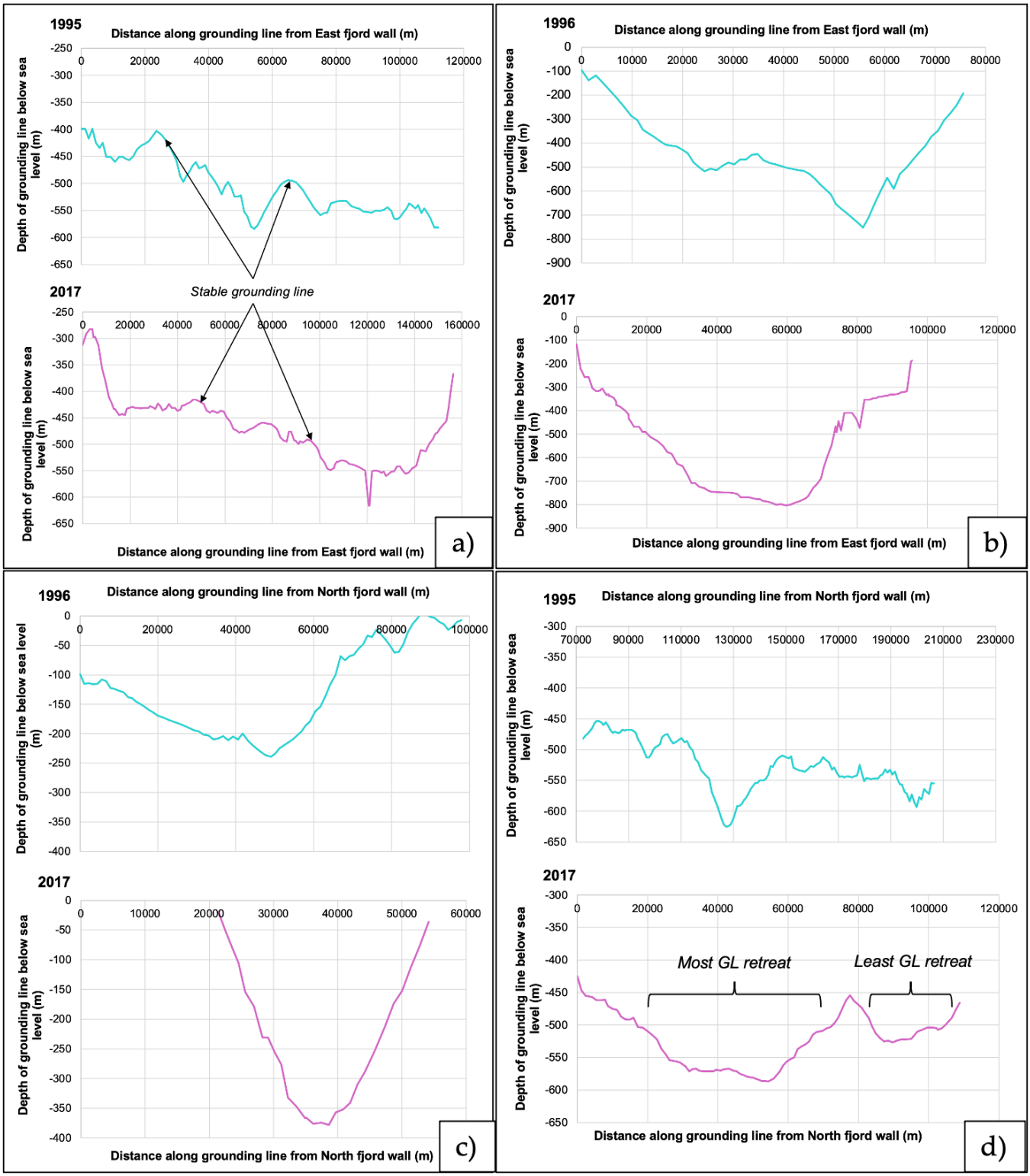

***Figure 9**: InSAR-derived grounding line profiles from BedMachine v3 data in 1995/6 (cyan) and 2017 (magenta) at a) Petermann Gletsjer, b) Ryder Gletsjer, c) Hagen Brae, d) Nioghalvfjerdsbræ. Key sections are annotated.*

4.1.3 Fjord geometry

Waters in the Nares strait in front of Petermann are generally quite shallow, but a very deep (at some points >1km) channel feeds deep waters to the grounding line. This can be seen in Figure 10a, which shows a deep channel running along Petermann Gletsjer's westerly fjord wall. The long profile associated with Figure 10a shows that the ice shelf is situated over a normal slope, behind which sits an overdeepening. The grounding line has retreated into this overdeepening between 1999 and 2016. At Ryder Gletsjer (fig. 10b), the entrance to the fjord is very shallow (< 300 m.b.s.l.), but just behind a sill at which the July terminus positions of 1997 and 2016 rest, a very deep (>1100 m.b.s.l.) trough, or overdeepening extends backwards to the grounding line locations. Beyond this point, bed elevation increases along a steep normal slope towards the overground inland portions of the fjord. At Hagen Brae (fig. 10c), the entrance to the fjord is even shallower, at just 50 m.b.s.l. Just in front of the 2016 terminus position, the bed deepens to around 350 m in a large trough, and then rapidly steepens to reach the surface. It should be noted that to the more northerly side of this centreline, a shallow channel resting below sea level with a normal slope continues inland for 100 km. At Nioghalvfjerdsbræ (fig. 10d), the entrance to the fjord is also much shallower than the main body, with the presence of a sill clearly visible just in front of the 1999 terminus position. The depth behind this point drops of rapidly to ~1200 m.b.s.l., before increasing gradually inland again over a gentle normal slope. Notably, none of the fjords have retrograde slopes extending beyond the current grounding line position.

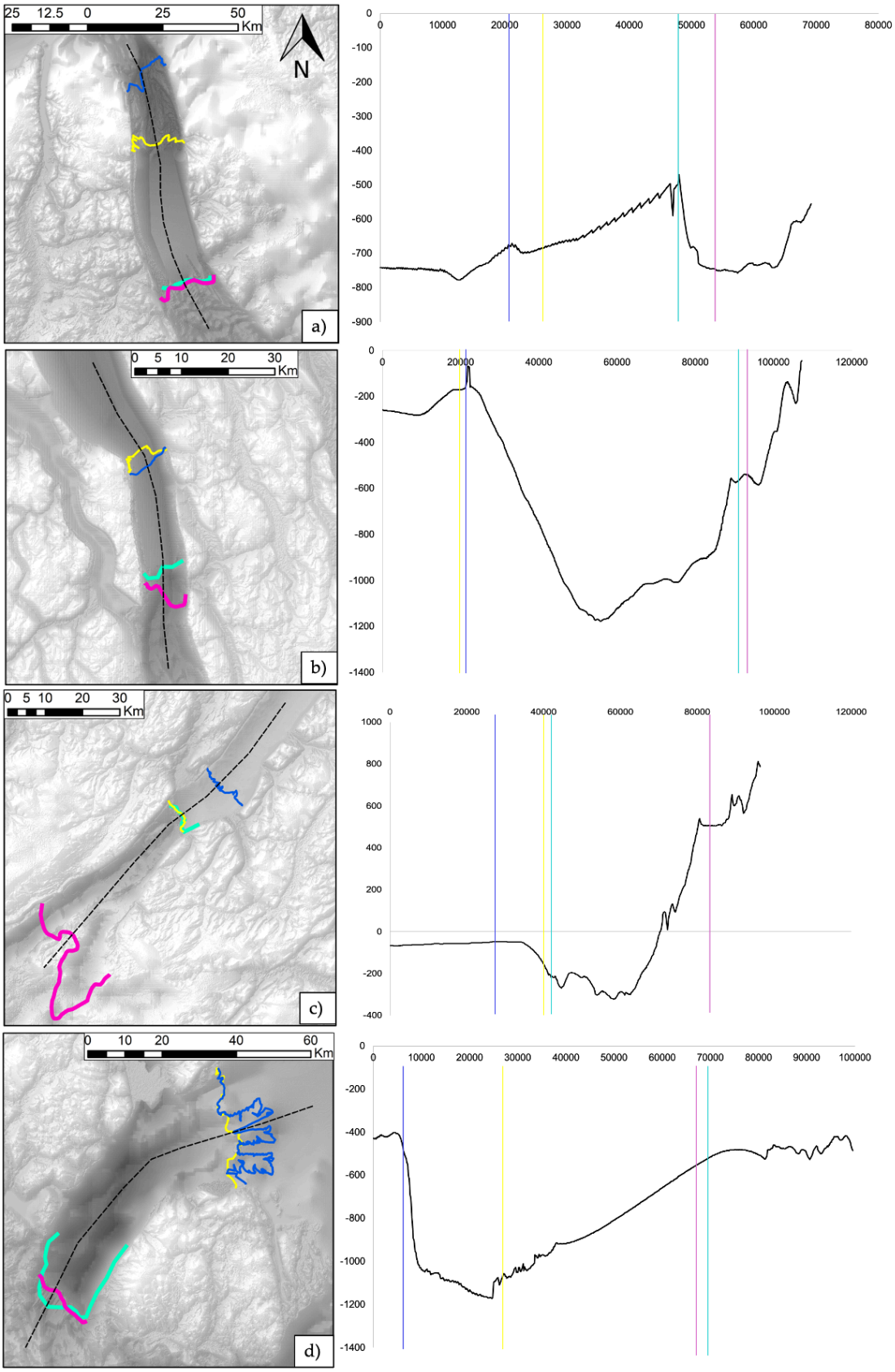

***Figure 10**: DEMs of bed topography and long profiles of fjords at a) Petermann Gletsjer, b) Ryder Gletsjer, c) Hagen Brae, d) Nioghalvfjerdsbræ. Black dashed lines show location of associated long profiles, all of which are plotted moving from downstream to upstream. For context, navy blue lines denote 2016 July terminus position, yellow lines first measured terminus position, cyan lines 1995/6 grounding line position, and magenta line 2016 grounding line positions. In graphs, x axis = distance along transect (m), and y axis = depth of fjord below sea level (m)*

4.1.4 Changes to terminus positions

An overview of average annual terminus positions in comparison to their last measured position (0 m) is shown in Figure 11. A map showing every measured terminus position included in the study is presented in Figure 12. All termini retreated over the study period, with Hagen Brae (plotted on secondary axis) undergoing the most significant change in position, and Ryder Gletsjer undergoing the least. Between 1999 and 2016, Petermann Gletsjer's terminus retreated by 30,128 m, at an average rate of 1768 m a^{-1}. Between 1999 and 2009, terminus position remained relatively stable, fluctuating within a ~4000 m window during several relatively small iceberg calving events. Between July and August of 2010, a major calving event resulted in a terminus retreat of more than 24,000 m. Following this, the terminus advanced by ~1600 m up to 2013, when a smaller calving event resulted in an average retreat of ~9,600 m. Between 2012 and the most recently measured position in 2016, the terminus re-

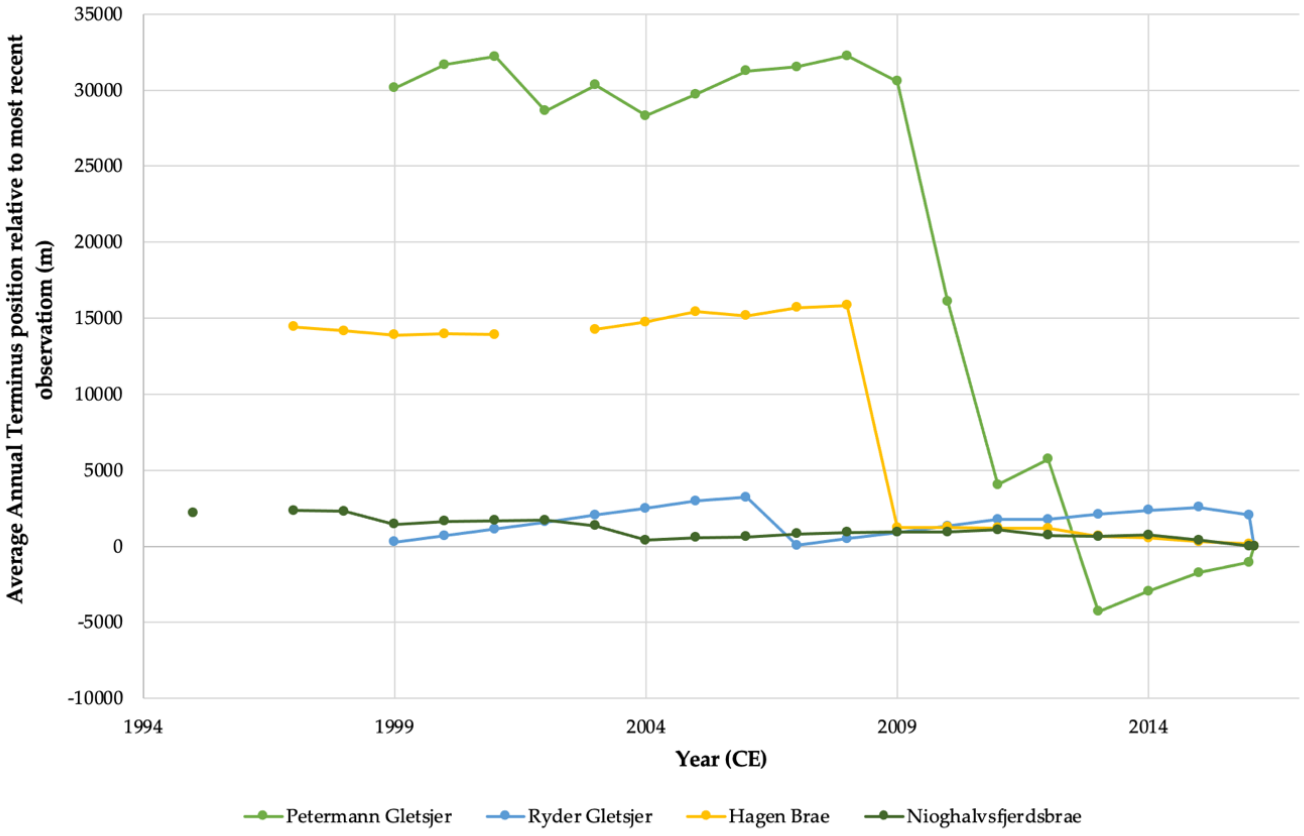

***Figure 11**: Average annual terminus position over time at each study site, relative to most recent observation (0). The most recent observation has been plotted at year = 2016.1 for context*

advanced by an average of just over 4000 m. At Petermann Gletsjer, measured retreat patterns of the terminus are roughly consistent across the width of the terminus. Positional terminus fluctuations became even more uniform following the major 2010 calving event.

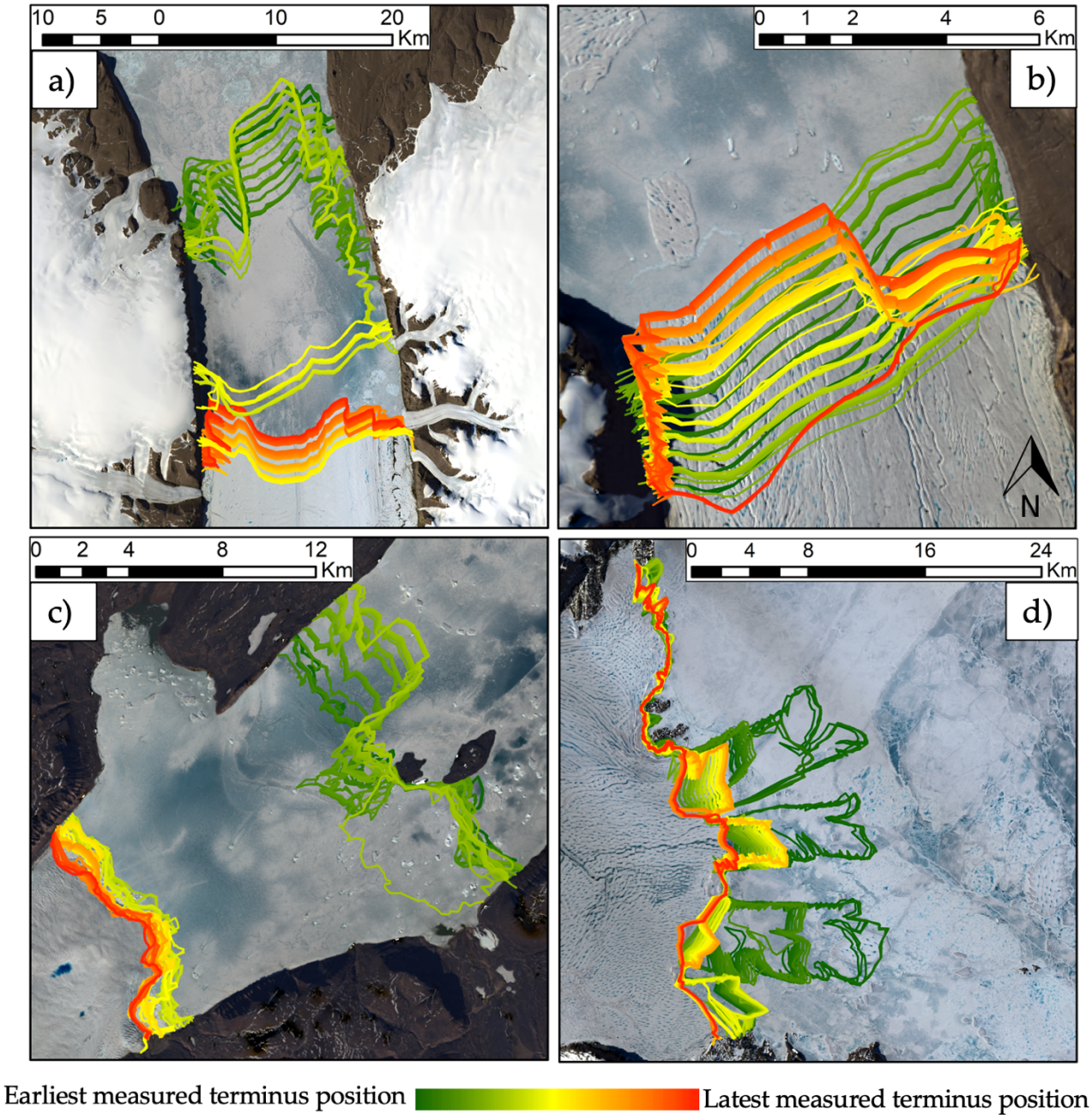

***Figure 12**: Mapped terminus positions superimposed over Landsat 8 imagery from July 2016 at a) Petermann Gletsjer, b) Ryder Gletsjer, c) Hagen Brae, d) Nioghalvfjerdsbræ. Each measurement is colour-coded according to date of acquisition.*

Ryder Gletsjer's terminus position in 1999 is just 285 m more advanced than the most recent observation resultant in an average retreat rate of 16 m a^{-1}, but between these observations the calving front has undergone two major cycles of advance and retreat. Between its initial position in 1999 and July 2006, Ryder Gletsjer's terminus advanced by 2928 m. The advance over this period was very consistent, at an average rate of ~ 418 m a^{-1}. Between July and August 2006, the calving front retreated to ~200 m behind its position in 1999 during a large calving event. From 2007 to 2015, the terminus re-gained 80 % of the ground lost during its 2006 calving event, maintaining consistent net increase in position despite several smaller calving events decreasing the extent of the eastern calving front during this period. The only exception to this annual advance was between 2011 and 2012, when one such calving event meant that the calving front underwent no net change despite over 400 m of advance along the central and western terminus. This pattern of advance with small calving events continued until late July 2016 (between the 19th and 24th), when another large calving event resulted in a retreat of 3069 m within less than five days. Advance and retreat patterns over the study period are approximately uniform amongst centrelines until 2012, when calving events began more frequently on the eastern portion, and the pattern of change in this region diverged from the central and western terminus (fig. 12b).

From 1997 to 2016, Hagen Brae's terminus retreated the furthest of all the study sites, migrating by 14,421 m, with a resultant average retreat rate of 759 m a^{-1}. However, 93% of this retreat took place during a single catastrophic calving event between observations in July 2008 and June 2009. Before this calving event, the terminus had been comparatively stable, advancing at an average rate of 128 m a^{-1}. After the calving event, the terminus continued its pattern of retreat at a much slower annual average rate of 174 m a^{-1}. The variation in retreat patterns across Hagen Brae is substantial during the pre-calving event period, with most of the average advance due to changes to the northern margin. During the same period, central and southerly portions of the calving front remained relatively stable or did not show a clear direction of change. Following the calving period, each centreline measured a trend

of retreat, and the pattern and magnitude of this change varied only slightly by position.

Nioghalvfjerdsbræ underwent retreat of 2,184 m between 1995 and 2016, at an average rate of 104 m a^{-1}. In contrast to Hagen Brae and Ryder Gletsjer – at which one to two major calving events were the primary control on average terminus position – Nioghalvfjerdsbræ's calving front variation is controlled by smaller, more frequent calving events along three protruding sections of the calving front (fig. 12d). Outside these areas, there is very little variation in terminus position over the study period, with centrelines outside the extended tongues measuring a maximum of ~ 1,300 m of variation in position over the study period, and in some cases, measuring less than 50 m total variation. Contrastingly, the range in terminus position along the protruding extensions reaches up to 12 km. The most significant calving events took place in 1999, 2004, 2013, and 2016, over the course of which the floating tongue extensions were lost completely. However, some of the mass lost after earlier calving events was briefly regained through gradual terminus re-advance but was not maintained, meaning that the last measured terminus position mapped the presence of no floating tongues.

4.1.5 Changes to ice shelf area

Maps showing first and last measured ice shelf extent at each glacier are presented in Figures 13 and 14. An overview of estimated changes to ice shelf area as percentage difference from the first measurement is shown in Figure 15. It should be noted that the grounding line positions used to constrain these areas are linearly interpolated, and so some aspect of the linear trend exhibited in these measurements is an artefact of the methodology. However, it is still considered a useful exercise within this study as it allows for the contextualisation of terminus changes by incorporating both the direction and magnitude of grounding line evolution into terminus observations.

Between the late 1990s and early July 2016, Petermann Gletsjer and Nioghalvfjerdsbræ lost 27% and 8% of their ice shelf area respectively, whilst Ryder Gletsjer and Hagen Brae gained an additional 28% and 180% respectively from their first ice shelf area measurement. The change in Petermann Gletsjer's ice shelf area was driven by a major calving event in 2010, during which nearly 1/3 of its ice shelf broke away. In the context of this significant change in calving front location over time, changes to the grounding line have played a comparatively small role in governing ice shelf area and location change between 1999 and 2016. Changes in Ryder Gletsjer's ice shelf area and location, in comparison to Petermann Gletsjer's, are influenced more strongly by grounding line retreat. This is particularly true in the eastern portion of the fjord, as early July terminus position in 1999 and 2016 are very similar (fig. 13). However, it should be noted that as the terminus position used to constrain ice shelf area is measured in early July, the major calving event which occurred in late July at Ryder Gletsjer bringing it to its most recently measured position occurred after the estimation of 2016 ice shelf area shown in Figure 13. This most recent measurement of terminus position is displayed as the deepest red digitised position in Figure 12b.

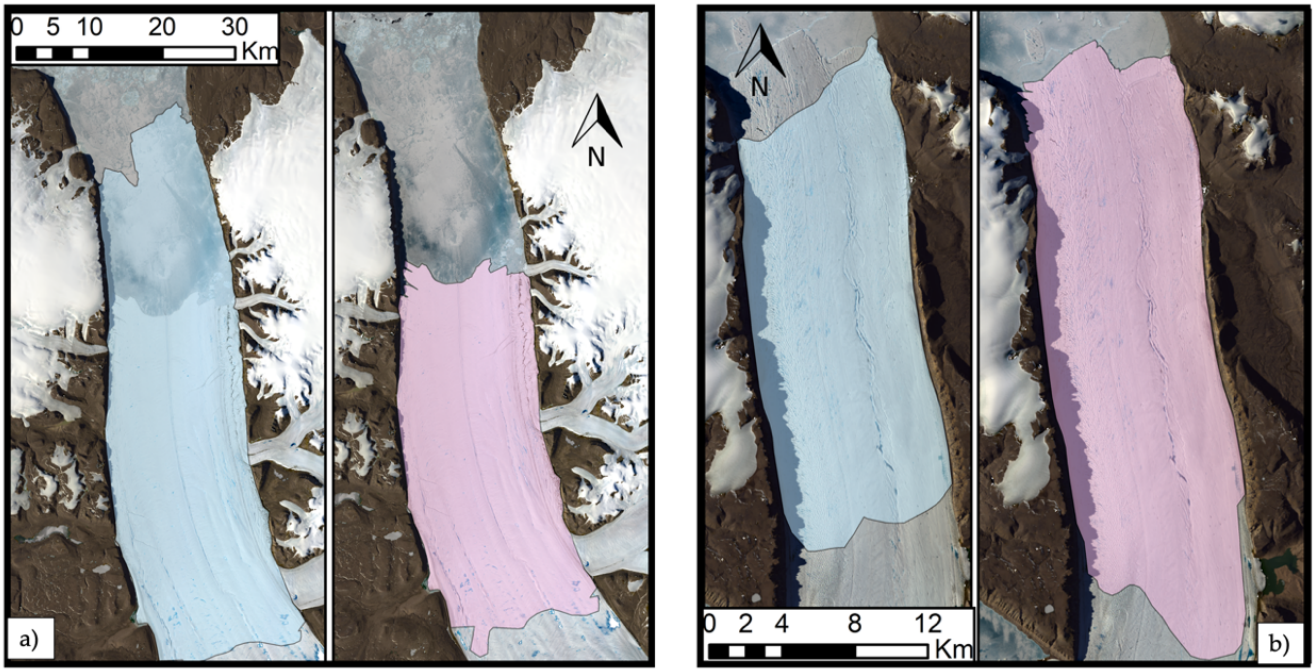

***Figure 13**: Mapped ice shelf extent in 1999 (blue) and 2016 (pink) at a) Petermann Gletsjer, and b) Ryder Gletsjer. Note different scales in each pair of images.*

Whilst Petermann and Ryder Gletsjer have undergone significant changes to their ice shelves but remain broadly in comparable locations, the Hagen Brae ice shelf is in an entirely different location in 2016 compared to its 1997 position. The terminus has retreated to such an extent that in 2016 it rests extremely close to the position of its 1997 grounding line. At Hagen Brae, grounding line change is the dominant cause of changes to ice shelf properties, retreating a distance more than 3 times that of the terminus over the study period. The extent of this change is visible in Figure 14a, in which the ice shelf location can be seen to be at completely different locations within the fjord, at first extending forwards from the location of the 1997 grounding line, and

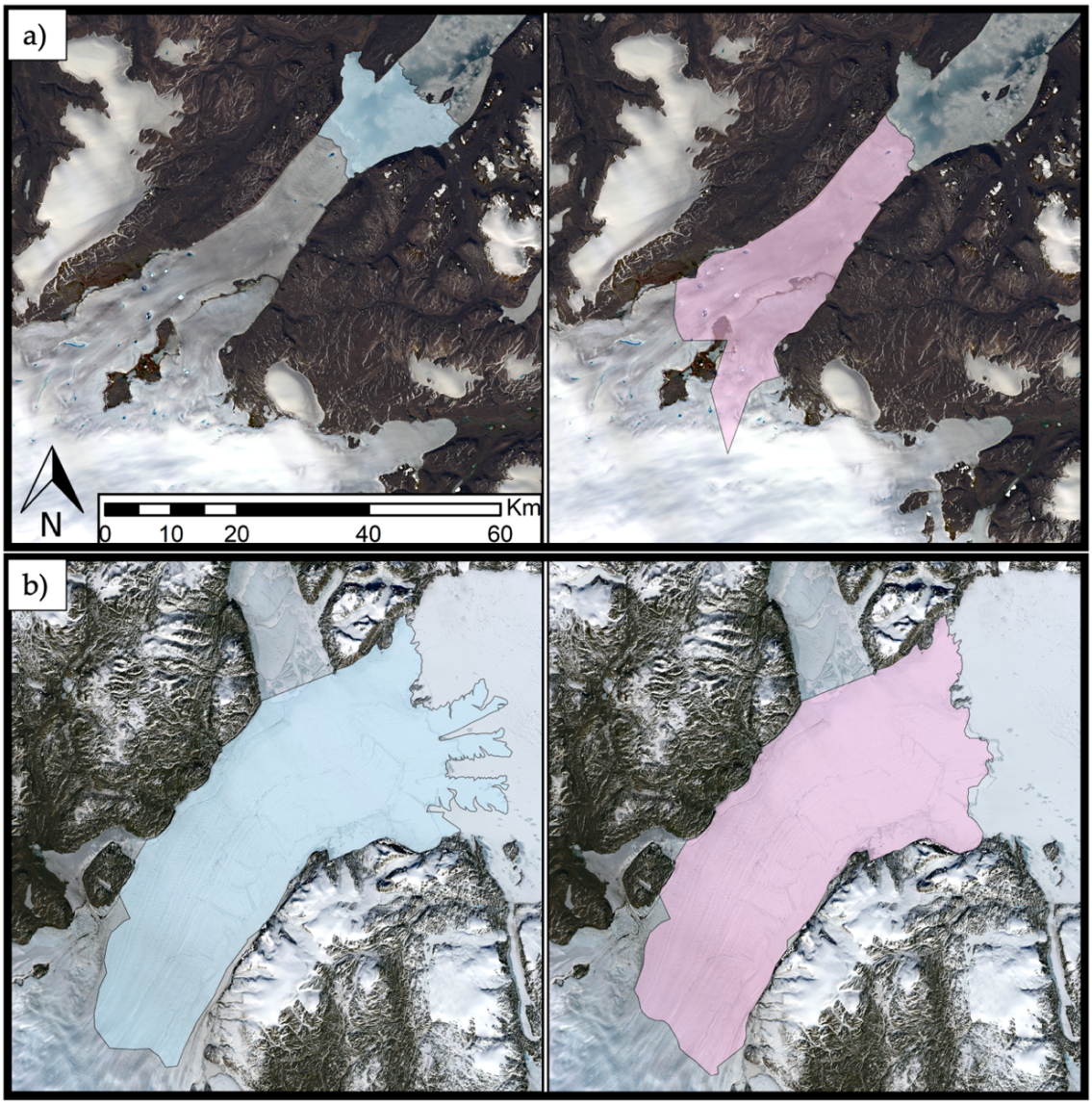

Figure 14: *Mapped ice shelf extent a) Hagen Brae in 1997 (blue) and 2016 (pink), and b) Nioghalvfjerdsbræ in 1995 (blue) and 2016 (pink). All images have the same scale and orientation.*

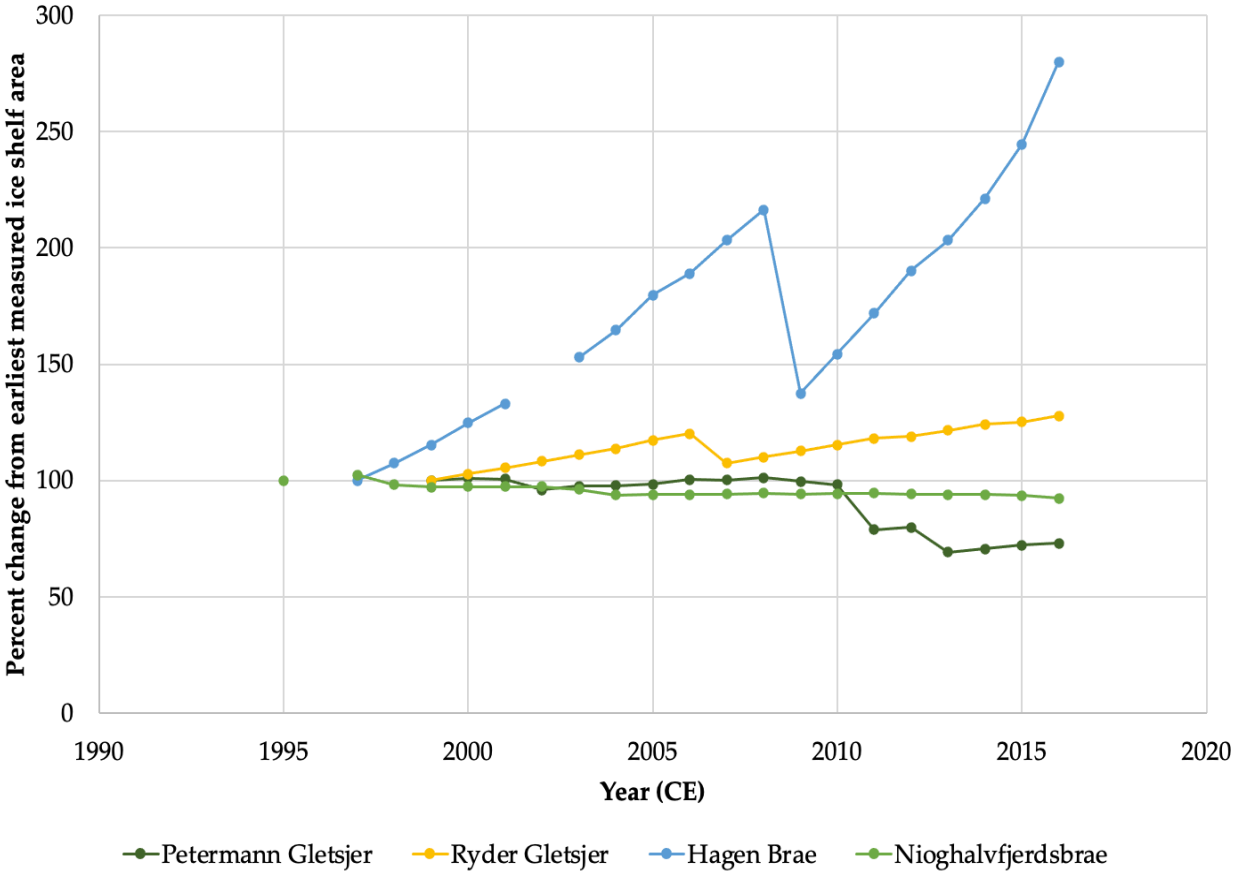

***Figure 15**: Graph showing percent change from earliest measured ice shelf area at each study site over time.*

then extending inland from this same point, now the location of the 2016 grounding line position.

Nioghalvfjerdsbræ's ice shelf underwent only one major change throughout the study period. It lost the three sections of its ice shelf which protrude from the calving front, all of which were of a greater area that that lost by a slight advance in grounding line position during the same period. This meant that terminus position, rather than grounding line position as at Hagen Brae, exerted most control over ice shelf area during the study period. Therefore, of the four study sites examined, ice shelf change at Petermann Gletsjer and Nioghalvfjerdsbræ can be considered to be a product primarily of terminus variation, whilst Ryder Gletsjer and Hagen Brae's ice shelves were influenced by both changes to their terminus position and the evolution of their grounding lines.

4.2 Environmental forcing factors

4.2.1 Runoff

Across all four study areas, annual cumulative runoff increased over the study period. Between 1995 and 2016, Petermann Gletsjer's runoff increased by 68%, Ryder Gletsjer's by 149%, Hagen Brae's by 223%, and Nioghalvfjerdsbræ's by 107%. In addition to this highly variable magnitude of change, the amount of runoff across each catchment varied significantly as a function of area, but the patterns of interannual fluctuation remained very similar (figure 16). Whilst small interannual variation in runoff was consistent across the study period, the interdecadal trend is clearly one of distinct increase. All catchments had peaks in runoff in 1998, 2003, 2005, 2008, and 2012. Petermann and Ryder Gletsjer's maximum cumulative runoff values were reached during 2012, at respective values of 7,323,787 kg/m^2 and 3,013,903 kg/m^2, whilst Hagen Brae and Nioghalvfjerdsbræ's runoff peaked in 2016 at 2,229,387 kg/m^2 and 6,441,157 kg/m^2 respectively. Minimum cumulative runoff values at Petermann Gletsjer (2,749,884 kg/m^2) and Hagen Brae (691,237 kg/m^2) occurred in 1996, and at Ryder Gletsjer (993,258 kg/m^2) in 1995, whilst the minimum annual runoff recorded at Nioghalvfjerdsbræ (1,932,587 kg/m^2) was in 2006.

Variation in runoff increases across the study wites is mapped in Figure 17. It shows that Ryder Gletsjer had the most uniform increase in runoff across the ice shelf area, whilst at Petermann Gletsjer the greatest increases in runoff were concentrated on the lower ice shelf and uppermost sections of the glacier. At Petermann Gletsjer's grounding line and along the western fjord wall, the runoff did not increase by as much as across other parts of the ice shelf and glacier. At Hagen Brae, runoff increased by greater magnitudes moving downstream, with the exception of the south-easterly fjord wall, along which the increase in runoff was not of as great a magnitude as across the rest of the ice shelf. Unlike the other study areas, runoff increase across Nioghalvfjerdsbræ is not concentrated along the ice shelf. Instead, the greatest increases in runoff were upstream from the grounding line, along a steep slope

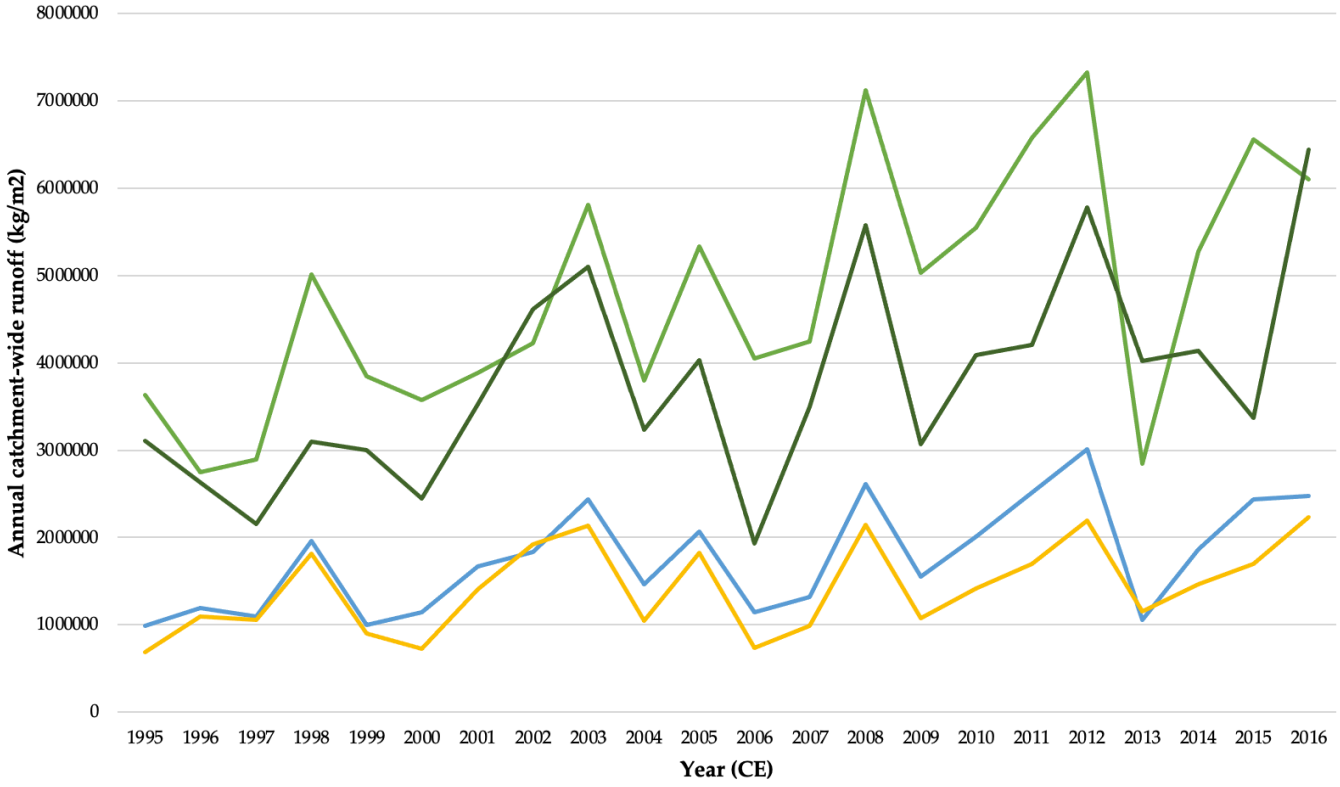

***Figure 16**: Graph showing changes in annual runoff at each study site over time.*

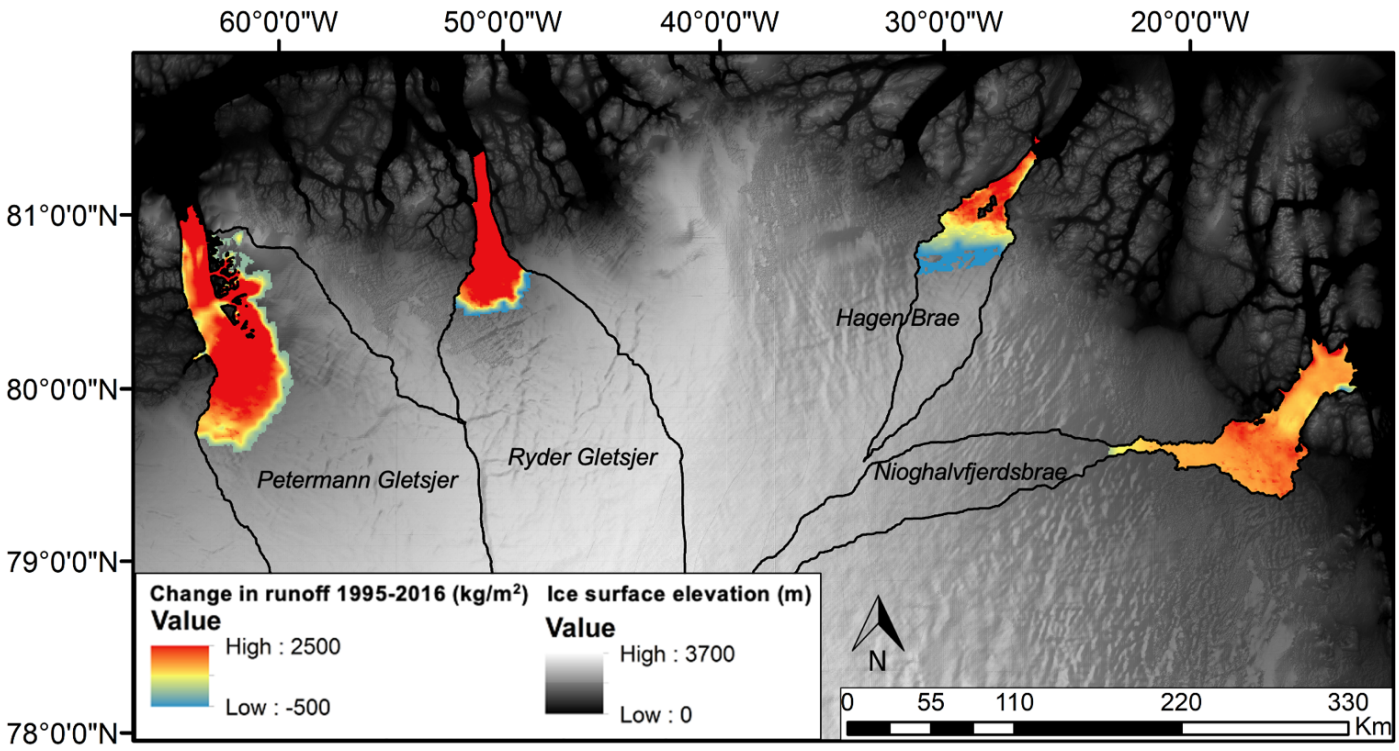

***Figure 17**: Map showing change in runoff across each grid square of RACMO runoff model between 1995 and 2016. Catchments of each glacier are outlined in black, and background values (0) are not displayed. Background image shows surface elevation from BedMachine v3 dataset.*

leading down to the ice shelf. Across the ice shelf, increase is relatively uniform across the central section, but increased slightly long the northerly fjord wall, and decreased in the most north-easterly corner.

4.2.2 Ocean Temperature

Surface water ocean temperatures (0-200 m deep) have also been in a phase of continuous increase over the study period, with increases of 0.26, 0.25, 0.17, and 0.27 °C between 1995 and 2016 at the waters in front of Petermann Gletsjer, Ryder Gletsjer, Hagen Brae, and Nioghalvfjerdsbræ respectively. At Petermann and Ryder Gletsjers, the increase in temperature over time was relatively smooth, whilst interannual variation has a greater magnitude at Hagen Brae and Nioghalvfjerdsbræ (Figure 19). The difference in ocean temperature between 1995 and 2016 is shown in figure 18.

Deep water temperatures (200-800 m) have increased across all study sites, but the variation in both the magnitude and pattern of this increase is much more substantial than those of surface water temperatures (Figure 20). Whilst deep waters at Nioghalvfjerdsbræ have increased in temperature by 0.58 °C in just two decades, increases in waters adjacent to Ryder Gletsjer and Hagen Brae were just 0.09 °C and 0.01 °C respectively over the same period: two orders of magnitude less than the increase at Nioghalvfjerdsbræ. Deep waters in the Nares Strait adjacent to Petermann Gletsjer increased by 0.15 °C over the study period. Deep water temperature at all study areas fell by > 0.1 °C between 1995 and 2005, and then increased by between 0.16 and 0.69 °C from 2006 to 2016. The most variation occurred at Nioghalvfjerdsbræ, where ocean temperatures rose rapidly between 1995 and 1997, fell to below 0 °C by 2002, stayed at around this level until 2005, then rapidly increased again to 0.90 °C over the following nine years.

Figure 18 shows that the increase in surface water temperature over the study period has been uniform across most of the water surrounding North Greenland, increasing at rates between 0 and 0.3 ˚C throughout most of the model pixels. The only

exceptions to this slow warming pattern have been off the coast of Nioghalvfjerdsbræ, where temperature increase exceeded 0.5 ˚C, and in the southerly portion of the Nares Strait, where warming approached 0.5 ˚C. It also confirms that the most distinct increases in deep ocean temperature, of up to 1.5 ˚C, have occurred along the north-easterly coast in front of Nioghalvfjerdsbræ fjord. This region is controlled by circulation of the East Greenland and Norwegian Atlantic current. Comparably, deep ocean temperatures across the rest of the study area have increased at a uniform rate of between 0 and 0.2, with the exception of a patch to the north of Ellesmere Island, which was subject to warming approaching 0.5 ˚C.

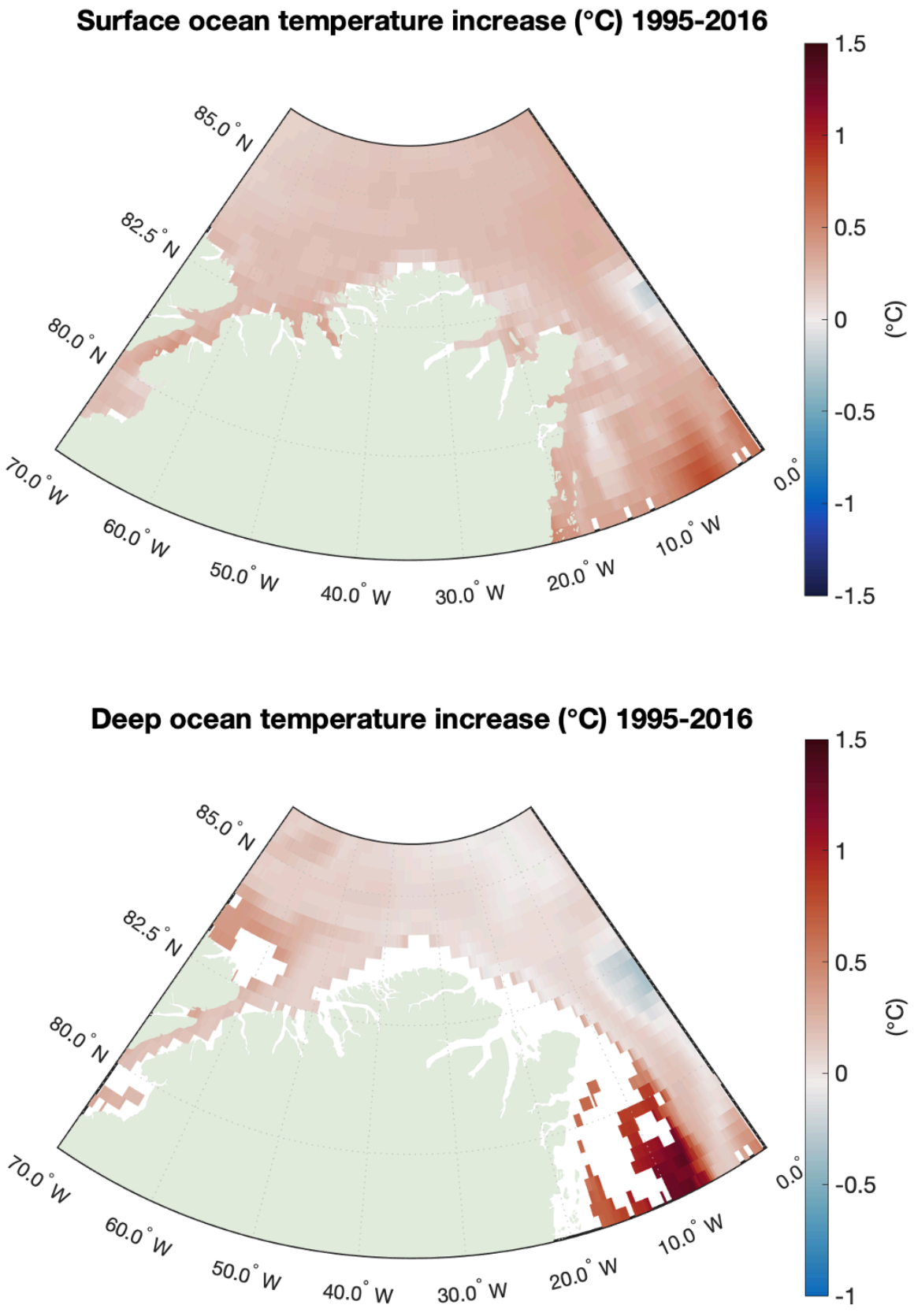

***Figure 18**: Map showing change in ocean temperature at each grid square of ensemble ocean model between 1995 and 2016 around North Greenland. Outline of Greenland and Ellesmere Island are shown in pale green. Surface and deep waters are defined as 0-200 m and 200-800 m below sea level respectively.*

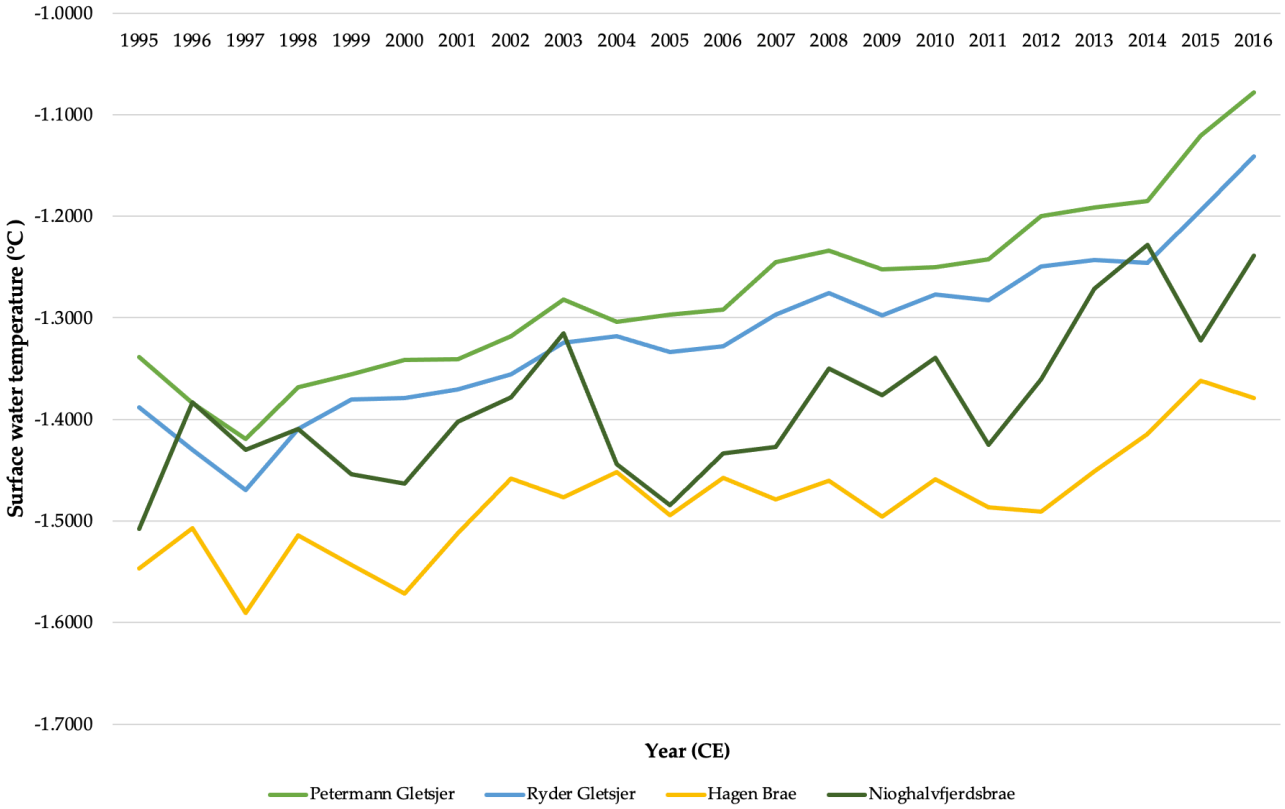

Figure 19: *Annual average surface-water temperature (0-200 m.b.s.l.) at each ocean study box between 1995 and 2016.*

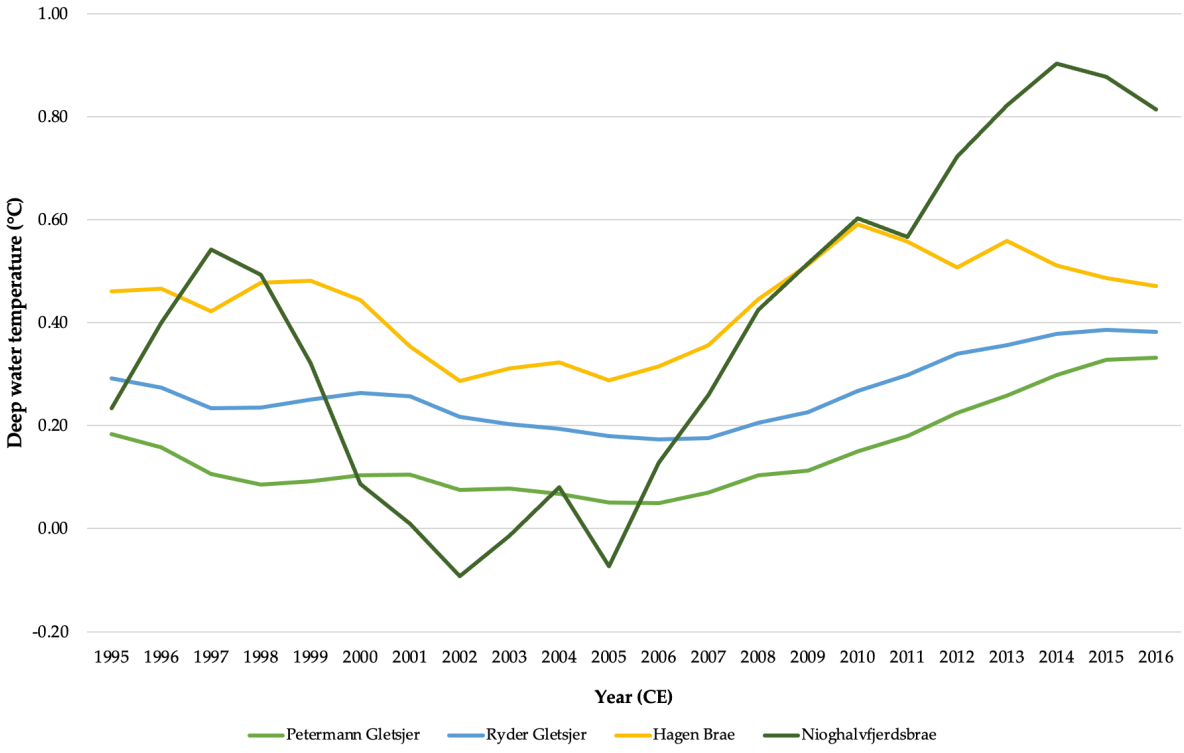

Figure 20*: Annual deep-water temperature (200-800 m.b.s.l.) at each ocean study box between 1995 and 2016.*

4.3 Statistical tests for linear relationships

4.3.1 Runoff

Of the four variables tested for correlation and cointegration with runoff (average annual terminus position at four study sites), the only statistically significant relationship between runoff and terminus position was found at Nioghalvfjerdsbræ. Correlation tests between runoff and terminus position found an R^2 value of 0.26 ($p = 0.02$), whilst p values for correlation between runoff and terminus position at other glaciers varied between 0.13 and 0.74. No cointegration was found between runoff and terminus position at any study area. All scatter plots where statistically significant results were established between average annual terminus position and runoff are shown in Figure 21. No outliers have been removed.

4.3.2 Ocean temperature

The average annual terminus position of Hagen Brae was found to have a statistically significant ($p < 0.01$) correlation with both surface-water and deep-water temperature, with R^2 values of 0.34 and 0.58 respectively. The average annual terminus position of Petermann Gletsjer also demonstrates a statistically significant ($p < 0.01$) correlation between both surface-water and deep-water temperature (0.68 and 0.88 R^2 values respectively). Ryder Gletsjer's annual terminus position does not have a statistically significant relationship with either surface- or deep-water temperature, Nioghalvfjerdsbræ has statistically significant correlations between surface-water temperature and average annual terminus position, but no significant correlation was found with deep-water temperature. An R^2 value of 0.29 was found when testing for correlation between surface-water temperature and average annual terminus position ($p = 0.01$). None of the average annual terminus positions was found to be co-integrated with either surface or deep-water temperature. All scatter plots where

statistically significant results were established between average annual terminus position and runoff are shown in Figure 21. No outliers have been removed.

4.3.3 Combined proxies

No statistically significant relationship was found between either the M_1 or M_2 parameterisations used by Cowton et al. (2018) and any study area's average annual terminus position. All statistical results are summarised in Table 3.

Petermann Gletsjer	**Runoff**	**Surface Temp**	**Deep Temp**	**M1**	**M2**
R2	0.13	**0.68**	**0.88**	0.03	0.05
P (correlation)	0.13	**< 0.01**	**< 0.01**	0.46	0.34
P (cointegration)	> .1	> .1	> .1	> .1	> .1
Ryder Gletsjer					
R2	0.01	0.00	0.00	0.01	0.01
P (correlation)	0.74	0.83	0.92	0.74	0.76
P (cointegration)	>.1	>.1	>.1	>.1	>.1
Hagen Brae					
R2	0.11	**0.34**	**0.58**	0.05	0.05
P (correlation)	0.15	**< 0.01**	**< 0.01**	0.36	0.33
P (cointegration)	>.1	>.1	0.06	>.1	>.1
Nioghalvfjerdsbræ					
R2	**0.26**	**0.29**	0.15	0.04	0.07
P (correlation)	**0.02**	**0.01**	0.07	0.38	0.22
P (cointegration)	>.1	>.1	>.1	>.1	>.1

***Table 3**: Summary of statistical results from tests for linear relationship between terminus position and environmental forcing factors. Statistically significant values have been displayed in bold. Note that acceptable p value was set at < 0.05,*

Petermann Gletsjer

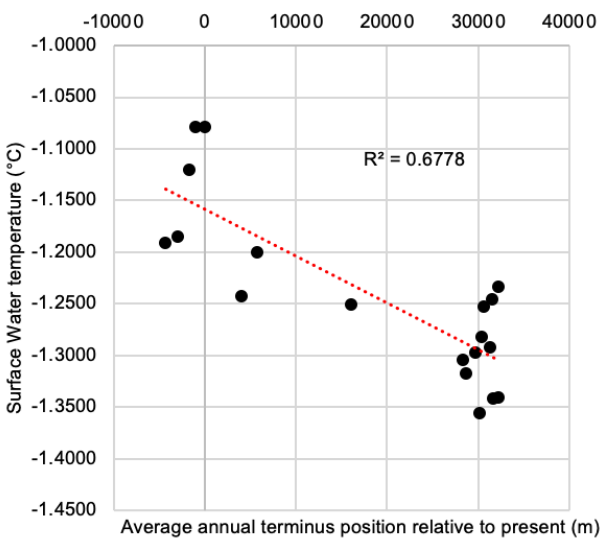

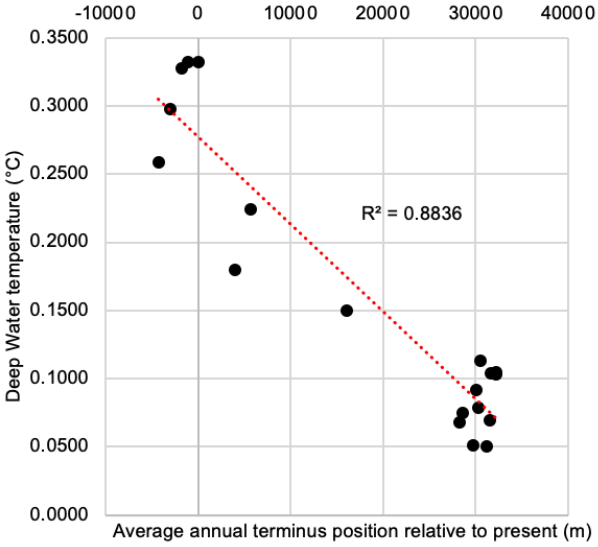

Hagen Brae

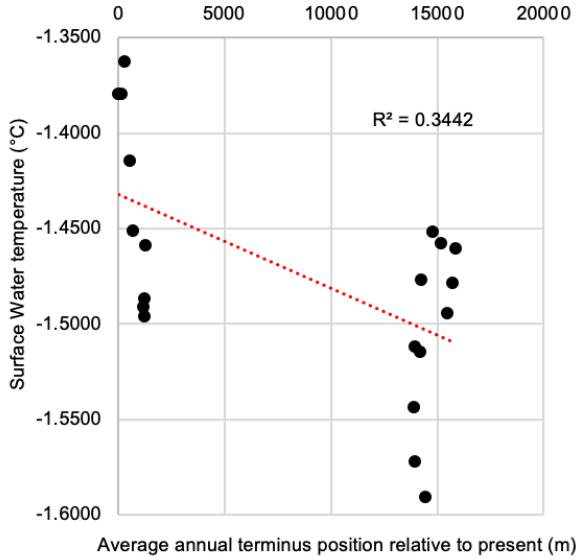

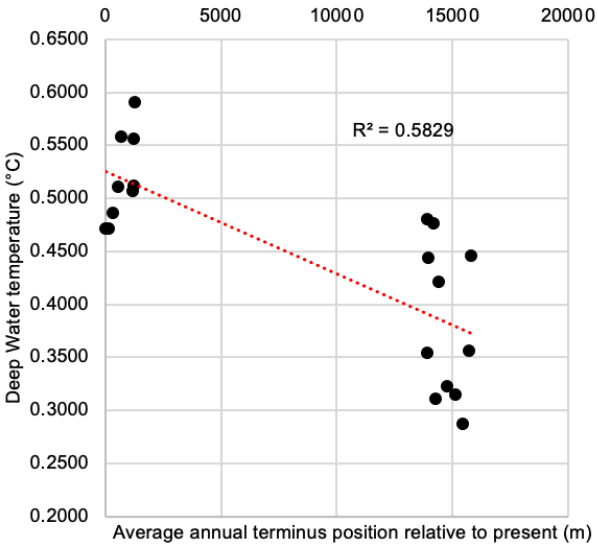

Nioghalvfjerdsbræ

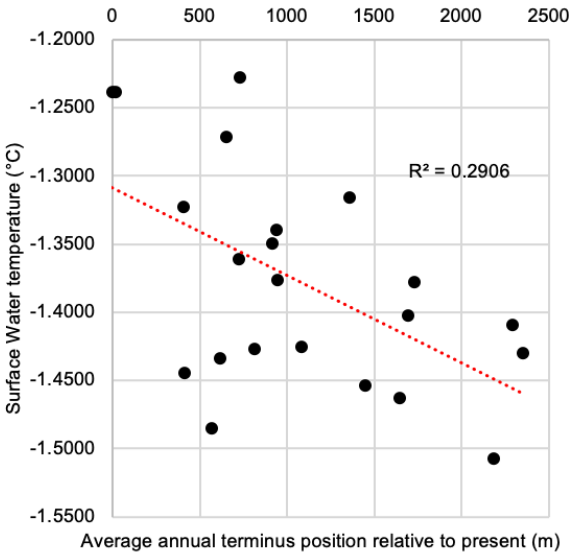

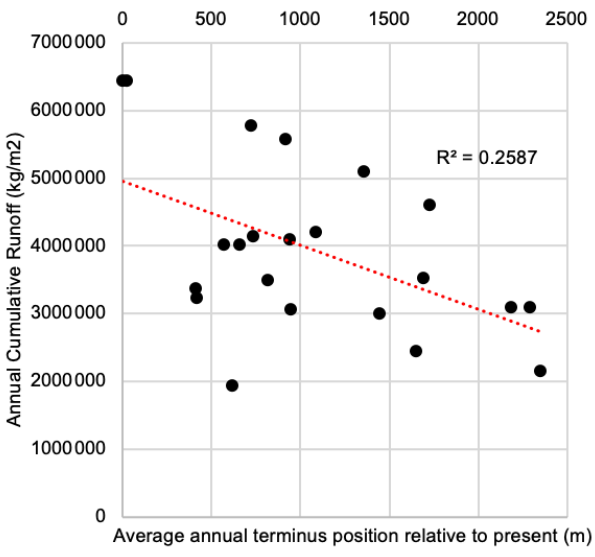

***Figure 21**: Scatter plots of linearly correlated relationships with statistical significance between average annual measurements of environmental variables and average annual terminus positions.*

5. Discussion

5.1 Changes to ice shelf area

Change in the properties of ice shelves across the region has been highly variable and does not follow a longitudinal gradient. Both Nioghalvfjerdsbræ and Petermann Gletsjer have shrunk by less than 30 % in ice shelf area over the study period, whilst Hagen Brae has nearly doubled in size due to comparatively moderate retreat of its terminus not keeping pace with the substantive retreat of its grounding line. The behaviour of these ice shelves are widely aligned with patterns of shrinkage and retreat which have been observed around the polar ice sheets as the climate warms (Baumhoer, et al., 2020; Slater, et al., 2021). Ryder Gletsjer is a notable outlier from this trend in that its ice shelf first gained in area slowly, and then underwent a sudden loss constituting around 12% of its total area; a pattern of advance and retreat which occurred twice in nearly identical patterns over the study period (fig. 11). This is in line with findings from Holmes, et al. (2021), who suggest that the behaviour of Ryder Gletsjer is cyclical and comparable to larger Antarctic ice shelves which calve large, tabular icebergs infrequently and are governed by internal glaciological stresses more so than their external thermal forcing (De Rydt, et al., 2019).

This has important consequences for ice dynamics, as a consistent, repetitive pattern of advance and retreat ostensibly implies an inherent stability within the ice shelf. However, this may not be the case, as Holmes et al. (2021) have postulated that 2017 upstream acceleration of ice may be a de-buttressing response to mass loss associated with the 2016 calving event, a response which was not present after the 2007 event, possibly indicating that the ice shelf's back stress has reduced past a critical point, through the combination of a major background calving event coinciding with enhanced thinning or structural damage. This pattern of change echoes those observed recently at Antarctic ice shelves, where flexure-induced collapse as a result of warming atmospheric temperatures and enhanced melt ponding has been found to

be responsible for a disruption of natural calving cycles at ice shelves such as Larsen B (Banwell, et al., 2013; Joughin & MacAyeal, 2005). More detailed observation at Ryder Gletsjer is required to fully understand whether a disruption is underway; specifically, a modelling assessment of the strength of the ice shelf and its response to the rapidly warming local meteorological and atmospheric conditions would be useful in testing this hypothesis.

5.2 Effect of environmental forcing factors

Ryder Gletsjer demonstrates no response to environmental variables, adding weight to the theory described above that it is subject to an internally, rather than externally modulated calving cycle. The presence of linear relationships between both shallow and deep ocean temperature and terminus position at Petermann Gletsjer and Hagen Brae suggests that oceanic forcing is having a strong influence on calving rates at these ice shelves. This conclusion at Petermann Gletsjer is supported by a series of recent papers produced both in response to the 2010/2012 calving events, and associated with the OMG project, which have previously drawn similar conclusions (Wood, et al., 2021; Hill, et al., 2018a; Münchow, et al., 2016), but much less work has been undertaken assessing ocean forcing at Hagen Brae. It is therefore of particular interest that so much of the variance at Hagen Brae can be explained by surface and deep-water temperature (34% and 58% respectively). The only major recent study at Hagen Brae (Solgaard, et al., 2020) has looked primarily at internal glaciological feedbacks rather than external factors, examining the effect of englacial meltwater accumulation on ice shelf behaviour. These results suggest more weight should be given to oceanic forcing as a driver of Hagen Brae's past and future ice shelf disintegration, especially if as Solgaard et al. suggest, the glacier's ice shelf will surge again into deeper and therefor warmer fjord waters once it has reached an equilibrium following the enormous loss in 2008/2009.

Nioghalvfjerdsbræ is the only glacier responding directly to atmospheric forcing, which indicates that the ambient temperatures along the East coast of Greenland are sufficient to induce near-terminus destabilisation of the ice shelf through either direct thinning, or other melt-induced mechanisms (section 2.2). This is supported by data from Hanna, et al. (2021), who show that summer and autumn temperature increases have been concentrated along the northeast coast, and particularly that summer atmospheric temperature increases are most pronounced close to Nioghalvfjerdsbrae (fig. 22). It is therefore considered highly likely that melt processes are playing a significant role in driving the loss of area from the Nioghalvfjerdsbrae ice shelf, and that if air temperatures along the North Greenland coast continue to increase, that other glaciers will become more susceptible to this mechanism of ice shelf destabilisation. Nioghalvfjerdsbræ is also responding to increases in surface water temperature but not deep water temperatures. It is possible that deep AW is being modified and cooled before reaching the terminus during its circulation within the fjord and resultant mixing with cool meltwater (Carroll, et al.,

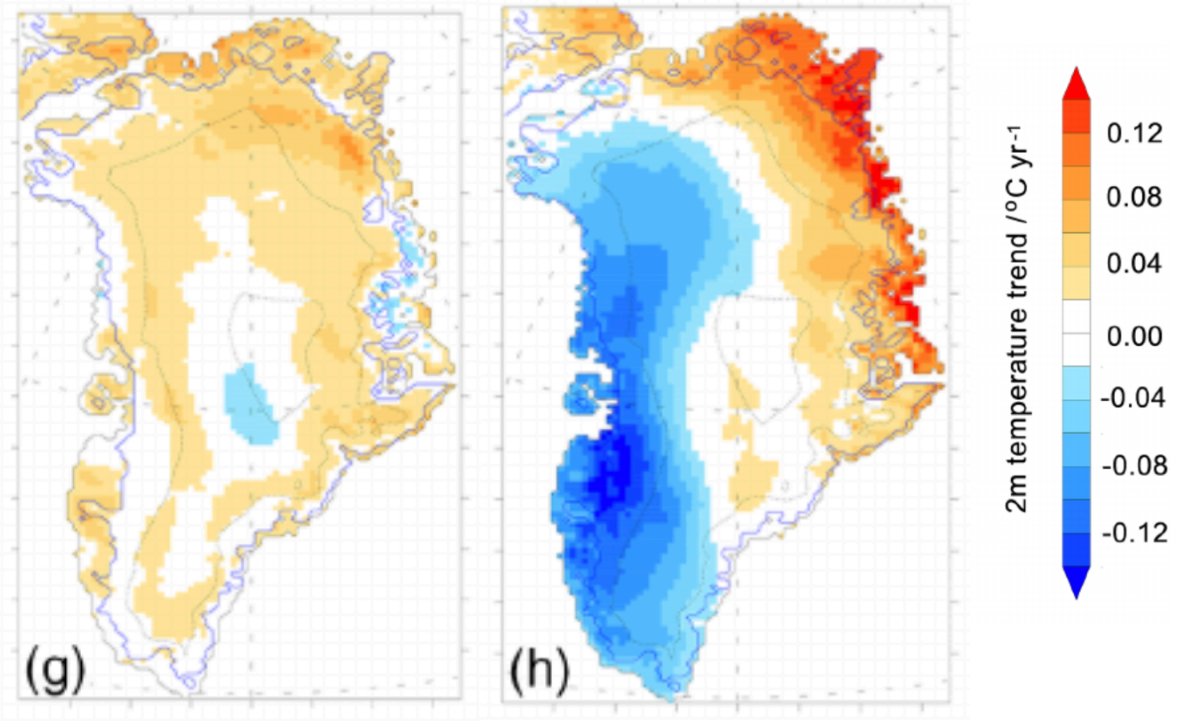

Figure 22: *Seasonal air temperature trends from 2000-2018 from Hanna, et al. (2021), showing summer (JJA - g) and autumn (SON – h) temperature trends, obtained from MAR and constrained using local weather station data.*

2018), or possible that the less typical pattern of deep water temperature change (fig. 20) at Nioghalvfjerdsbræ, with a major cooling between 1997 and 2010 not observed at any other study site is disrupting the relationship. This unusual and unexpected pattern in the context of globally increasing ocean temperatures (Cheng, et al., 2019) may be a result of a shift in dynamics of the East Greenland Current. Våge et al. (2018) suggest that a 21st century cooling of this water mass may be a feedback from a shrinking ice coverage along the East Greenland coast, as enhanced convection on a wider shelf area in conjunction with Ekman transport towards the continent allows for mixing of cooler fresh polar waters at the top of the column with underlying AW. If this is the case, continued retreat of Nioghalvfjerdbræ could induce a negative feedback through which warming of the deep waters in front of its fjord are suppressed, in turn depressing oceanic thermal forcing at Nioghalvfjerdsbræ's terminus. However, this mechanism does not seem particularly likely to be in effect given that following the cooling event, deep water temperatures rapidly rebounded to exceed all other study sites by 2016.

It is an unexpected finding that Petermann Gletsjer is not also responding to annual variations in surface runoff, as the magnitude and rate of increase of runoff across its catchment are nearly aligned with those at Nioghalvfjerdsbrae (fig. 16). A possible explanation for this this may be that as the calculated catchment for Petermann Gletsjer in this study is over four times greater than Nioghalvfjerdsbrae's, the melt running across its surface will be less concentrated on its ice shelf, and a large portion of this may be making its way to the bed via supraglacial lake drainage or moulins upstream of the ice shelf (Selmes, et al., 2011). Whilst this melt may eventually be transported to the grounding line where it has the potential to induce plume melting, it may be stored englacially for some time beforehand (Kendrick, et al., 2018) potentially delaying the response. Better distributed or englacially stored meltwater may also reduce the likelihood of ponding on the ice shelf surface, and the weakening of the Petermann ice shelf from above may be limited in this manner. Another explanation may be that efficient transport of melt across the ice shelf itself is limiting

the effect of meltwater injection and subsequent plume formation at the grounding line. Macdonald, et al. (2018) have suggested that this process may be underway at Petermann, due to the characterisations of meltwater drainage patterns across the front of the ice shelf.

It should be noted that Rosier, et al. (2019) found melt-induced basal cracks to be present at the grounding line, so whilst there may be no observable linear response to melt in the terminus record, this is not a guarantee that a threshold of melt may be surpassed as summer temperatures continue to increase, resulting in the further loss of large portions of Petermann Gletsjer's ice shelf to through-crevassing, initiated and propagated by excesses of meltwater.

5.3 Applicability of linear forcing framework to ice shelf environments

The co-integrated linear relationship established between environmental forcing parameters and terminus position at tidewater glaciers by Cowton et al. (2018), is not present at North Greenland ice shelves, which shows that the factors governing terminus retreat of glaciers with floating ice shelf components are modulated by additional factors not included in the statistical analysis undertaken in this study, and which do not have a controlling influence on grounded tidewater glaciers. Importantly, this implies that the linear relationships between terminus position and ocean temperature currently used within ISMIP6 sea level projections (Nowicki, et al., 2016) inherently flawed, and likely contributing to inaccuracies in the forecasts of patterns and rates of sea level rise. However, linear relationships are present between the rate of terminus change and tested environmental variables at three out of four study sites. The outlier from this – Ryder Gletsjer – contrasts with the other glaciers in that it displays no linear direction of change in its terminus position and no relationship to any of the tested forcing factors, likely because it is instead in a cycle of consistent background calving and regrowth at a periodicity of ~ 10 years as discussed above. The linear relationships which are present imply that whilst

terminus position at Petermann Gletsjer, Hagen Brae, and Nioghalvfjerdsbrae are not responding in an integrated manner with environmental variables, some degree of their deterioration is certainly being forced in simple terms by increasing ocean and atmosphere temperatures. Petermann Gletsjer shows the most conclusive of these linear relationships, with 88% of the variation in its terminus over the study period explained by ocean temperature between 200 and 800m. Neither of the combined forcing parameterisations returned positive results for correlation or cointegration, which emphasises how different the processes occurring at North Greenland ice shelves are from the more simplistic linear relationships observed at grounded tidewater glaciers draining the ice sheet. Specifically, it is suggested that geometry is modulating the response of the ice shelves to oceanic and atmospheric warming, and controlling the calving cycle observed at Ryder Gletsjer, as discussed in section 5.4.

5.4 Geometry and stability of North Greenland ice shelves

The bathymetry of each ice shelf is thought to explain much of the variation in consistency of response to environmental forcing, and the lack of co-integration between terminus position and environmental variation. It is suggested that the cyclical nature of Ryder Gletsjer's evolution is governed by its bathymetry, specifically by a pronounced overdeepening with a sill close to the entrance of the fjord, clearly visible in Figure 10. This sill corresponds to the position of maximum terminus advance at any time during the study period, and during both calving cycles once the terminus reaches this point, a major calving event is initiated. This implies that once the terminus reaches the far side of the sill, further advance is unsustainable, and a collapse is initiated, likely due to critical values of strain within the ice shelf being surpassed. Petermann Gletsjer's distinct susceptibility to ocean forcing is also thought to be influenced by its fjord geometry. This is primarily because it has a very deep channel which helps warm AW to bypass the sill and destabilise the terminus through melting from below. In contrast, Hagen Brae (which does not respond as strongly to

deep water temperature increase at an R^2 of 0.58 compared to Petermann's 0.88) has no such channel, and so the transport of AW into its fjord will take place more slowly, via leakage over the sill rather than direct funnelling. At Nioghalvfjerdsbræ, deep waters are also blocked by bathymetry surrounding the fjord entrance which rarely exceeds 200 m.b.s.l., and so the deep water temperatures sampled on the continental shelf, away from the fjord entrance are not guaranteed to be entering the fjord. This is one explanation for why it is not correlated with variation in deep water temperature.

As well as providing insight into previously observed behaviour, profiles of fjord bathymetry can give an indication as to the future stability of the glaciers. Ryder Gletsjer and Hagen Brae grounding lines are currently resting on bathymetric highs, which indicates that their terminus position has the potential to remain relatively stable for some time. Petermann Gletsjer and Nioghalvfjerdsbrae both rest on prograde slopes, but not at pinning points, and so whilst there is potential for retreat of these sections, it is also possible that their retreat will be slowed by the stabilising effect of retreat along prograde slopes. Catania, et al. (2018) give weight to this hypothesis as they suggest that glacial retreat will conclude once grounding lines reach the back of overdeepenings. Notably, the back of overdeepenings of each of the study glaciers are all within one ice shelf length of the current grounding line position, placing a limit on the potential future retreat of these ice shelves. Hagen Brae's 2016 grounding line is located in front of a trough which extends several 10s of kms inland below the glacier, and rests below sea level. Though it is on a normal slope, the intrusion of warm ocean water to the subglacial environment via this trough would have enormous potential to initiate acceleration, thinning and enhanced discharge from Hagen Brae in much the same way as has been occurring at glaciers in the Amundsen Sea embayment, and is hypothesised to drive future retreat of the West Antarctic Ice Sheet (Walker, et al., 2007; Seroussi, et al., 2017).

It is possible that the geometry of the ice shelves themselves are also modulating their response to environmental forcing, and in particular to runoff. Much of near-terminus zones of the Petermann and Ryder Gletsjer ice shelves are barely

connected to the fjord walls, as they have extensive damage to their margins. Hill, et al. (2018b) suggest that the very suppressed velocity response at Petermann to 2010/2012 calving events may be due to reduced tensile strength of the ice shelf having already initiated a de-buttressing through heavy damage to the ice-marginal portions. They suggest instead that once the ice shelf has retreated into more intact ice, that an increased velocity to de-buttressing will be more pronounced. Damage at the margins is of additional concern, as if meltwater is becoming concentrated at the fjord walls where damage is present, there is more potential for stress to propagate backwards through the ice shelf and induce terminus retreat according to work from Cowton et al. (2019), introduced in section 2.3. Lhermitte et al. (2020) also note that damages to ice shelves in their shear, marginal zones have the potential to pre-condition them for retreat, through positive feedbacks initiated when shearing along margins results in weakening of ice shelf back stress, with a subsequent increase in velocity resulting in enhanced rates of shear. Although their study is focussed on Antarctic ice shelves, it is not inconceivable that this process could also occur at any of the four sites examined in this study. In fact, as Greenlandic ice shelves tend to be narrower than those in the Antarctic, any shear zone damage will compose a greater proportion of the overall ice shelf, which may result in a stronger feedback system that outlined in Lhermitte et al.'s study.

North Greenland glaciers ice shelves will not initiate mass loss from the interior of the ice sheet on the scales hypothesised in Antarctica if MISI is initiated, however, that is not to say that the dynamic mass losses from thinning and acceleration feedbacks have less potential to induce sea level rise in the order of several cms. In comparison to Antarctic glaciers, the GrIS is also responding to much warmer air and ocean temperatures, and so should be considered highly vulnerable to extensive mass loss, even though major instabilities in the ice sheet such as MISI are much more likely to occur across Antarctica. This section has outlined several ways in which these study sites have the potential to enter unstable phases of retreat in response to local geometry, internal glaciological feedbacks, and external climate variables.

5.5 Limitations of methodology

This methodology has several limitations, firstly that loss of ice shelf mass from submarine melt and thinning is not included, which certainly has the potential to exert a control on ice shelf behaviour (Wilson, et al., 2017). Secondly, that the limited availability of grounding line positions and subsequent need for linear interpolation means that interannual variation in ice shelf area were only approximated, and any sudden changes within the study period were not captured. This is not considered to be a major limitation at grounding lines which have undergone relatively little change over the study period (Petermann, Ryder, and Nioghalvfjerdsbrae), as terminus position will be the primary control on areal change at these glaciers, however it is a source of potential significant error at Hagen Brae, which underwent much more extensive grounding line retreat. It is considered highly possible that the retreat pattern of Hagen Brae's ice shelf area was in reality much less gradual than implied by Figure 15. Instead, it is likely that Hagen Brae's grounding line underwent most of its retreat following major destabilisation of the ice shelf during the 2008/9 calving event. The exact pace of retreat between the 1997 and 2017 grounding line positions cannot be calculated due to lack of InSAR grounding line data. However, it could be hypothesised due to the overdeepening between the 1997 position and the bathymetric high point at which the grounding line currently rests (fig. 10), that the grounding line retreated rapidly through this overdeepening before coming to rest at its 2017 position several years before measured. This pattern of retreat has been recreated in modelling studies by Pattyn, et al. (2019), but it is also possible that the extensive retreat of the grounding line lagged behind Hagen Brae's major calving event. Evidence for a lag in grounding line retreat following de-buttressing during deglaciation from the last glacial maximum has been found in the foraminiferal record (Bart, et al., 2018), and recreated in numerical modelling studies (Goldberg, et al. 2009).

5.6 Future study

This study highlights in particular the need for more concentrated efforts to improve the temporal resolution of historic North Greenland grounding line positions measured through differential interferometry. Without such a record, the behaviour of ice shelves buffering against significant rises to GMSL cannot be understood or quantified in their entirety, and predictions of their future behaviour will be consequently limited. Grounding line behaviour is a vastly important component, and without these measurements, it is impossible to thoroughly consider whether the linear parameterisations of grounding line forcing employed in ISMIP6 is accurate, or introducing significant error as the highly locally variable results of this study suggest. It is suggested that more resources are invested in developing automated processing of SAR imagery, to help overcome the time-consuming nature of grounding line measurement. The satellite record between 1995 and 2017 contains data which could be converted into grounding line positions to help fill in the gaps in the record, particularly at Hagen Brae, so that fine-resolution grounding line migration can be included in model hindcasting. Notably this includes the TanDEM-X program which has coverage beginning from the launch of the second twin satellite in 2010, and ASAR sensor onboard Envisat – operational from 2002 to 2012.

Additionally, it is suggested that more work should focus on Hagen Brae's response to ocean forcing, as comparatively to the other glaciers examined throughout this study it has been understudied, and this thesis has established a statistically significant link between warming surface and deep ocean temperature, and Hagen Brae's retreat. Given that the changes to Hagen Brae's ice shelf have been the most dramatic of all the study sites, that together with neighbouring Academy Glacier it drains nearly 2% of the GrIS, and that the northern fjord has a trough extending inland with potential for future retreat, it is an obvious candidate for extensive future research.

6. Conclusions

Ice shelves along the North Greenland coast are of great significance to researchers as they provide a buttressing and stabilising effect for glaciers which drain a combined 13.6% of the GrIS (study glaciers). The specifics of their response to climate change and calving patterns are not well understood, which is introducing uncertainty into ice sheet models attempting to constrain predictions of future sea level rise. As several glaciers with floating ice shelves at more southerly latitudes in Greenland and across the Nares Strait on Ellesmere Island have undergone collapse or disintegration in recent years, great attention has been paid by the scientific community to the stability of the Arctic's few remaining ice shelves. This study has examined changes to four North Greenland ice shelves, with a primary aim of better understanding the extent to which they are vulnerable to local increases in ocean temperature and ice sheet runoff. Between the late 1990s and July 2016, Petermann Gletsjer was found to have lost 27% of its ice shelf area, and Nioghalvfjerdbrae 8%. Ryder Gletsjer increased its mass between the first and last annual measurements by 28% but returned to a nearly identical area as in the late 1990s following a major calving event in summer 2016. Hagen Brae increased in area by 180%, as relatively moderate retreat of its terminus was outpaced by grounding line retreat of over 51 km.

North Greenland's climatic conditions underwent a dramatic shift over the two-decade study period, with ice shelf runoff increasing across all study periods from a minimum of 68% at Petermann Gletsjer to a maximum of 223% at Hagen Brae. The only glacier which showed a statistically significant response to this increase was Nioghalvfjerdsbræ, which it is hence suggested is the only study site where ambient temperatures are sufficient to induce near-terminus destabilisation of the ice shelf. This is likely due to a concentration of 21st century warming at the northeast corner or Greenland, and as temperatures continue to increase across the continent, it is highly plausible that the other study sites will also cross this threshold within the coming decades. On average, surface ocean temperatures (between 0-200 m.b.s.l.) across the

study sites increased by just under 0.24 °C from 1995 to 2016. The average annual terminus positions of Petermann Gletsjer, Hagen Brae and Nioghalvfjerdsbrae are found to be correlated with these increases in surface temperature. Deep water temperatures (200-800 m.b.s.l.) also increased across all study sites, though at Ryder Gletsjer and Hagen Brae these increases were by less than 0.1 °C between 1995 and 2016, whilst Petermann Gletsjer and Nioghalvfjerdsbræ were subject to warming of 0.15 °C and 0.58 °C respectively between these years. Only the terminus positions of Petermann Gletsjer and Nioghalvfjerdsbræ were correlated with deep water temperature, with a particularly significant (88%) of terminus variation at Petermann controlled by deep water temperature. It is thought that this is due to the presence of a deep (> 1000 m) subglacial channel at its bed, which funnels warm AW to the underside of the glacier, and allows for destabilisation of the ice shelf from below. The average annual terminus position of Ryder Gletsjer was not found to be correlated with either ocean temperature or surface runoff, and it is suggested that its behaviour is instead governed by a combination of internal glaciological stresses and the underlying bathymetry (a ~1200 m overdeepening with a pronounced sill). These factors in conjunction have led to a stable and consistent calving cycle with a periodicity of ~ 10 years, which may be beginning to exhibit signs of disruption.

The secondary aim of testing whether the linear forcing framework established by Cowton, et al. (2018) and others at marine terminating outlets is applicable to glaciers with ice shelves at their termini was also achieved, and this study found that no co-integrated linear forcing exists. This raises severe limitations with current models used in sea level predictions, which use linear approximations to forecast the response of glaciers with ice shelves to ocean forcing. However, strong correlations were established between increasing ocean temperature and terminus retreat at Petermann Gletsjer and Hagen Brae, implying that these ice shelves are responding strongly to ocean thermal forcing, but with locally specific factors modulating this response, which are not exerting a significant influence on the retreat of grounded tidewater glacier margins. These localised, non-linear responses must be better

accounted for in future modelling studies. This study has synthesised and contributed to work on the stability of North Greenlandic ice shelves, although it should be noted that without improved temporal resolution of grounding line measurements, modellers will struggle to accurately project the future contribution of North Greenland as tests for the accuracy of linear forcing mechanisms currently included in modelling cannot be undertaken.

Reference List

Adusumilli, S. et al., 2020. Interannual variations in meltwater input to the Southern Ocean from Antarctic ice shelves. *Nature Geoscience,* 13(9), pp. 616-620.

An, L. et al., 2021. Ocean melting of the Zachariae Isstrøm and Nioghalvfjerdsfjorden glaciers, northeast Greenland. *Proceedings of the National Academy of Sciences,* 118(2).

Antoniades, D. et al., 2011. Holocene dynamics of the Arctic's largest ice shelf. *Proceedings of the National Academy of Sciences,* 108(47), pp. 18899-18904.

Arthur, J. et al., 2021. The triggers of the disaggregation of Voyeykov Ice Shelf (2007), Wilkes Land, East Antarctica, and its subsequent evolution. *Journal of Glaciology,* pp. 1-19.

Banwell, A. et al., 2014. Supraglacial lakes on the Larsen B ice shelf, Antarctica, and at Paakitsoq, West Greenland: a comparative study. *Annals of Glaciology,* 55(66).

Banwell, A., MacAyeal, D. & Sergienko, O., 2013. Breakup of the Larsen B Ice Shelf triggered by chain reaction drainage of supraglacial lakes. *Geophysical Research Letters,* 40(22), pp. 5872-5876.

Barrett, K., 2020. *The Bellagio of the natural world: glacial fountains.* [Online] Available at: https://oceanbites.org/the-bellagio-of-the-natural-world-glacial-fountains/ [Accessed 4 June 2021].

Bart, P. et al., 2018. A centuries-long delay between a paleo-ice-shelf collapse and grounding-line retreat in the Whales Deep Basin, eastern Ross Sea, Antarctica. *Scientific Reports,* 8(12392).

Bassis, J. & Ma, Y., 2015. Evolution of basal crevasses links ice shelf stability to ocean forcing. *Earth and Planetary Science Letters,* Volume 409, pp. 203-211.

Baumhoer, C. et al., 2020. Driving Forces of Circum-Antarctic Glacier and Ice Shelf Front Retreat over the Last Two Decades. *The Cryosphere Discussions.*

Benn, D., Cowton, T., Todd, J. & Luckman, A., 2017. Glacier Calving in Greenland. *Current Climate Change Reports,* 3(4), pp. 282-290.

Bevis, M. et al., 2019. Accelerating changes in ice mass within Greenland, and the ice sheet's sensitivity to atmospheric forcing. *Proceedings of the National Academy of Sciences,* 116(6), pp. 1934-1939.

Bjørk, A., Kruse, L. & Michaelson, P., 2015. Brief communication: Getting Greenland's glaciers right – a new data set of all official Greenlandic glacier names. *The Cryosphere,* 9(6), pp. 2215-2218.

Cabanes, C. et al., 2013. The CORA dataset: validation and diagnostics of in-situ ocean temperature and salinity measurements. *Ocean Science,* 9(1).

Carr, J., Vieli, A. & Stokes, C., 2013. Influence of sea ice decline, atmospheric warming, and glacier width on marine-terminating outlet glacier behavior in northwest Greenland at seasonal to interannual timescales. *Journal of Geophysical Research: Earth Surface,* 118(3), pp. 1210-1226.

Carroll, D. et al., 2018. Subannual and Seasonal Variability of Atlantic-Origin Waters in Two Adjacent West Greenland Fjords. *Journal of Geophysical Research: Oceans,* 123(9), pp. 6670-6687.

Carroll, D. et al., 2016. The impact of glacier geometry on meltwater plume structure and submarine melt in Greenland fjords. *Geophysical Research Letters,* 43(18), pp. 9739-9748.

Catania, G. et al., 2020. Future Evolution of Greenland's Marine-Terminating Outlet Glaciers. *Journal of Geophysical Research: Earth Surface,* 125(e2018JF004873).

Catania, G. et al., 2018. Geometric Controls on Tidewater Glacier Retreat in Central Western Greenland. *Journal of Geophysical Research: Earth Surface,* 123(8), pp. 2024-2038.

Cheng, L. et al., 2019. 2018 Continues Record Global Ocean Warming. *Advances in Atmospheric Sciences,* 36(3), pp. 249-252.

Choi, Y., Morlighem, M., Rignot, E. & Wood, M., 2021. Ice dynamics will remain a primary driver of Greenland ice sheet mass loss over the next century. *Communications Earth & Environment,* 2(26).

Christoffersen, P., O'Leary, M., Van Angelen, J. & van den Broeke, M., 2012. Partitioning effects from ocean and atmosphere on the calving stability of Kangerdlugssuaq Glacier, East Greenland. *Annals of Glaciology,* 53(60), pp. 249-256.

Cohen, J. et al., 2020. Divergent consensuses on Arctic amplification influence on midlatitude severe winter weather. *Nature Climate Change,* 10(1), pp. 20-29.

Cook, A. et al., 2016. Ocean forcing of glacier retreat in the western Antarctic Peninsula. *Science,* 353(6296), pp. 283-286.

Cowton, T. et al., 2018. Linear response of east Greenland's tidewater glaciers to ocean/atmosphere warming. *Proceedings of the National Academy of Sciences,* 115(31), pp. 7907-7912.

Cowton, T., Todd, J. & Benn, D., 2019. Sensitivity of Tidewater Glaciers to Submarine Melting Governed by Plume Locations. *Geophysical Research Letters,* 46(20), pp. 11219-11227.

Dawson, G. & Bamber, J., 2017. Antarctic Grounding Line Mapping From CryoSat-2 Radar Altimetry. *Geophysical Research Letters,* 44(23), pp. 11,886-11,893.

De Rydt, J., Gudmundsson, G., Nagler, T. & Wuite, J., 2019. Calving cycle of the Brunt Ice Shelf, Antarctica, driven by changes in ice shelf geometry. *The Cryosphere,* 13(10), pp. 2771-2787.

DeBeer, C. & Sharp, M., 2007. Recent changes in glacier area and volume within the southern Canadian Cordillera. *Annals of Glaciology,* Volume 46, pp. 215-221.

DeConto, R. & Pollard, D., 2016. Contribution of Antarctica to past and future sea-level rise. *Nature,* 531(7596), pp. 591-597.

Desportes, C. et al., 2019. *Quality Information Document for Global Ocean Reanalysis Multi-model Ensemble Products GREP GLOBAL-REANALYSIS-PHY-001-031.* [Online] Available at: https://resources.marine.copernicus.eu/?option=com_csw&view=details&product_id=GLOBAL_REANALYSIS_PHY_001_031 [Accessed 23 April 2021].

Dowdeswell, J., 2017. Eurasian Arctic Ice Shelves and Tidewater Ice Margins. In: L. Copland & D. Mueller, eds. *Arctic Ice Shelves and Ice Islands.* Dordrecht: Springer Netherlands, pp. 55-74.

Dowdeswell, J. & Jeffries, M., 2017. Arctic Ice Shelves: An Introduction. In: L. Copland & D. Mueller, eds. *Arctic Ice Shelves and Ice Islands.* Dordrecht: Springer Netherlands, pp. 3-21.

Eisermann, H. et al., 2020. Bathymetry Beneath Ice Shelves of Western Dronning Maud Land, East Antarctica, and Implications on Ice Shelf Stability. *Geophysical Research Letters,* 47(12).

Enderlin, E. et al., 2014. An improved mass budget for the Greenland ice sheet. *Geophysical Research Letters,* 41(3), pp. 866-872.

Engle, R. F. & Granger, C. W. J., 1987. Co-Integration and Error-Correction: Representation, Estimation, and Testing.. *Econometrica,* Volume 55, p. 251–276.

Esteban, M. et al., 2020. Adaptation to sea level rise: Learning from present examples of land subsidence. *Ocean & Coastal Management,* 189(104852).

Fahrner, D. et al., 2021. Linear response of the Greenland ice sheet's tidewater glacier terminus positions to climate. *Journal of Glaciology,* pp. 1-11.

Favier, L., Pattyn, F., Berger, S. & Drews, R., 2016. Dynamic influence of pinning points on marine ice-sheet stability: a numerical study in Dronning Maud Land, East Antarctica. *The Cryosphere,* 10(6), pp. 2623-2635.

Felikson, D. et al., 2017. Inland thinning on the Greenland ice sheet controlled by outlet glacier geometry. *Nature Geoscience,* 10(5), pp. 366-369.

Fenty, I. et al., 2016. Oceans Melting Greenland: Early Results from NASA's Ocean-Ice Mission in Greenland. *Oceanography,* 29(4), pp. 72-83.

Fricker, A. et al., 2009. Mapping the grounding zone of the Amery Ice Shelf, East Antarctica using InSAR, MODIS and ICESat. *Antarctic Science,* 21(5), pp. 515-532.

Fricker, H. et al., 2002. Redefinition of the Amery Ice Shelf, East Antarctica, grounding zone. *Journal of Geophysical Research: Solid Earth,* 107(B52092).

Fricker, H. & Padman, L., 2002. Tides on Filchner-Ronne Ice Shelf from ERS radar altimetry. *Geophysical Research Letters,* 29(1622).

Fricker, H. & Padman, L., 2006. Ice shelf grounding zone structure from ICESat laser altimetry. *Geophysical Research Letters,* 33(L15502).

Friedl, P. et al., 2018. Recent dynamic changes on Fleming Glacier after the disintegration of Wordie Ice Shelf, Antarctic Peninsula. *The Cryosphere,* 12(4), pp. 1347-1365.

Friedl, P., Weiser, F., Fluhrer, A. & Braun, M., 2020. Remote sensing of glacier and ice sheet grounding lines: A review. *Earth-Science Reviews,* 201(102948).

Goelzer, H. et al., 2020. The future sea-level contribution of the Greenland ice sheet: a multi-model ensemble study of ISMIP6. *The Cryosphere,* 14(9), pp. 3071-3096.

Goldberg, D., Holland, D. & Schoof, C., 2009. Grounding line movement and ice shelf buttressing in marine ice sheets. *Journal of Geophysical Research: Earth Surface,* 114(F04026).

Goldstein, R., Engelhardt, H., Kamb, B. & Frolich, R., 1993. Satellite Radar Interferometry for Monitoring Ice Sheet Motion: Application to an Antarctic Ice Stream. *Science,* 262(5139), pp. 1525-1530.

Good, S., Martin, M. & Rayner, N., 2013. EN4: Quality controlled ocean temperature and salinity profiles and monthly objective analyses with uncertainty estimates. *Journal of Geophysical Research: Oceans,* 118(12), pp. 6704-6716.

Gounou, A., Drévillon, M. & Clavier, M., 2020. *Product User Manual for Global Ocean Reanalysis Products GLOBAL-REANALYSIS-PHY-001-031.* [Online] Available at: https://resources.marine.copernicus.eu/?option=com_csw&view=details&product_id=GLOBAL_REANALYSIS_PHY_001_031 [Accessed 23 April 2021].

Gudmundsson, G., 2019. Instantaneous Antarctic ice sheet mass loss driven by thinning ice shelves. *Geophysical Research Letters,* 46(23), pp. 13903-13909.

Hanna, E. et al., 2021. Greenland surface air temperature changes from 1981 to 2019 and implications for ice-sheet melt and mass-balance change. *International Journal of Climatology,* 41(S1), pp. E1336-E1352.

Hewitt, I., 2020. Subglacial Plumes. *Annual Review of Fluid Mechanics,* 52(1), pp. 145-169.

Hill, E., Carr, J., Stokes, C. & Gudmundsson, G., 2018a. Dynamic changes in outlet glaciers in northern Greenland from 1948 to 2015. *The Cryosphere,* 12(10), pp. 3243-3263.

Hill, E., Gudmundsson, G., Carr, J. & Stokes, C., 2018b. Velocity response of Petermann Glacier, northwest Greenland, to past and future calving events. *The Cryosphere,* 12(12), pp. 3907-3921.

Hogg, A. et al., 2018. Mapping ice sheet grounding lines with CryoSat-2. *Advances in Space Research,* 62(6), pp. 1191-1202.

Holland, P., Feltham, D. & Jenkins, A., 2007. Ice Shelf Water plume flow beneath Filchner-Ronne Ice Shelf, Antarctica. *Journal of Geophysical Research: Oceans,* 112(C5).

Holmes, F. et al., 2021. Calving at Ryder Glacier, Northern Greenland. *Journal of Geophysical Research: Earth Surface,* 126(e2020JF005872).

Jakobsson, M. et al., 2020. Ryder Glacier in northwest Greenland is shielded from warm Atlantic water by a bathymetric sill. *Communications Earth & Environment,* 1(45).

Joughin, I. & MacAyeal, D., 2005. Calving of large tabular icebergs from ice shelf rift systems. *Geophysical Research Letters,* 32(L02501).

Kendrick, A. et al., 2018. Surface Meltwater Impounded by Seasonal Englacial Storage in West Greenland. *Geophysical Research Letters,* 45(19), pp. 10,474-10,481.

Kjær, H. et al., 2021. Recent North Greenland temperature warming and accumulation. *The Cryosphere Discussions.*

Kulp, S. & Strauss, B., 2019. New elevation data triple estimates of global vulnerability to sea-level rise and coastal flooding. *Nature Communications,* 10(4844).

Lea, J., 2018. The Google Earth Engine Digitisation Tool (GEEDiT) and the Margin change Quantification Tool (MaQiT) – simple tools for the rapid mapping and quantification of changing Earth surface margins. *Earth Surface Dynamics,* 6(3), pp. 551-561.

Lea, J., Mair, D. & Rea, B. R., 2014. Evaluation of existing and new methods of tracking glacier terminus change. *Journal of Glaciology,* 60(220), pp. 323-332.

Lellouche, J. et al., 2013. Evaluation of global monitoring and forecasting systems at Mercator Océan. *Ocean Science,* 9(1), pp. 57-81.

Lenaerts, J. et al., 2017. Meltwater produced by wind–albedo interaction stored in an East Antarctic ice shelf. *Nature Climate Change,* 7(1), pp. 58-62.

Lewis, S. & Smith, L., 2009. Hydrologic drainage of the Greenland Ice Sheet. *Hydrological Processes,* 23(14), pp. 2004-2011.

Lhermitte, S. et al., 2020. Damage accelerates ice shelf instability and mass loss in Amundsen Sea Embayment. *Proceedings of the National Academy of Sciences,* 117(40), p. 24735–24741.

Liu, Y. et al., 2015. Ocean-driven thinning enhances iceberg calving and retreat of Antarctic ice shelves. *Proceedings of the National Academy of Sciences,* 112(11), pp. 3263-3268.

Lowry, D. et al., 2019. Deglacial grounding-line retreat in the Ross Embayment, Antarctica, controlled by ocean and atmosphere forcing. *Science Advances,* 5(eaav8754).

Münchow, A., Padman, L. & Fricker, H., 2014. Interannual changes of the floating ice shelf of Petermann Gletscher, North Greenland, from 2000 to 2012. *Journal of Glaciology,* 60(221), pp. 489-499.

Münchow, A., Padman, L., Washam, P. & Nicholls, K., 2016. The Ice Shelf of Petermann Gletscher, North Greenland, and its connection to the Arctic and Atlantic Oceans. *Oceanography,* 29(4), pp. 84-95.

Macdonald, G., Banwell, A. & MacAyeal, D., 2018. Seasonal evolution of supraglacial lakes on a floating ice tongue, Petermann Glacier, Greenland. *Annals of Glaciology,* 59(76), pp. 56-65.

Machguth, H. et al., 2016. Greenland surface mass balance observations from the ice sheet ablation area and local glaciers. *Journal of Glaciology,* 62(235), pp. 861-887.

MacLachlan, C. et al., 2015. Global Seasonal forecast system version 5 (GloSea5): a high-resolution seasonal forecast system. *Quarterly Journal of the Royal Meteorological Society,* 141(689), pp. 1072-1084.

McConnochie, C., Cenedese, C. & McElwaine, J., 2020. Surface Expression of a Wall Fountain: Application to Subglacial Discharge Plumes. *Physical Oceanography,* Volume 50, pp. 1245-1263.

Millan, R. et al., 2018. Vulnerability of Southeast Greenland Glaciers to Warm Atlantic Water From Operation IceBridge and Ocean Melting Greenland Data. *Geophysical Research Letters,* 45(6), pp. 2688-2696.

Minchew, B. et al., 2018. Modeling the dynamic response of outlet glaciers to observed ice-shelf thinning in the Bellingshausen Sea Sector, West Antarctica. *Journal of Glaciology,* 64(244), pp. 333-342.

Moon, T., 2014. *Greenland outlet glacier behavior during the 21st century: Understanding velocities and environmental factors.* Seattle, Wash.: Earth and Space Sciences, Univ. of Washington.

Morlighem, M. et al., 2017. BedMachine v3: Complete Bed Topography and Ocean Bathymetry Mapping of Greenland From Multibeam Echo Sounding Combined With Mass Conservation. *Geophysical Research Letters,* 44(21), pp. 11,051-11,061.

Mouginot, J. et al., 2019. Forty-six years of Greenland Ice Sheet mass balance from 1972 to 2018. *Proceedings of the National Academy of Sciences,* 116(19), pp. 9239-9244.

Mouginot, J. et al., 2015. Fast retreat of Zachariæ Isstrøm, northeast Greenland. *Science,* 350(6266), pp. 1357-1361.

Moyer, A. et al., 2019. Spatio-temporal variations in seasonal ice tongue submarine melt rate at a tidewater glacier in southwest Greenland. *Journal of Glaciology,* 65(252), pp. 523-530.

Nagler, T., Forsberg, R. & Engdahl, M., 2018. *Product User Guide (PUG) for the Greenland_Ice_Sheet_cci project of ESA's Climate Change Initiative, version 2.2.* [Online] Available at: http://www.esa-icesheets-greenland-cci.org/ [Accessed 22 February 2021].

Nagler, T. et al., 2015. The Sentinel-1 Mission: New Opportunities for Ice Sheet Observations. *Remote Sensing,* 7(7), pp. 9371-9389.

Nick, F. et al., 2012. The response of Petermann Glacier, Greenland, to large calving events, and its future stability in the context of atmospheric and oceanic warming. *Journal of Glaciology,* 58(208), pp. 229-239.

Noël, B., van de Berg, W., Lhermitte, S. & van den Broeke, M., 2019. Rapid ablation zone expansion amplifies north Greenland mass loss. *Science Advances,* 5(eaaw0123).

Noël, B. et al., 2018. Modelling the climate and surface mass balance of polar ice sheets using RACMO2 – Part 1: Greenland (1958–2016). *The Cryosphere,* 12(3), pp. 811-831.

Nowicki, S. et al., 2016. Ice Sheet Model Intercomparison Project (ISMIP6) contribution to CMIP6. *Geoscientific model development,* 9(12), pp. 4521-4545.

Orsi, A. et al., 2017. The recent warming trend in North Greenland. *Geophysical Research Letters,* 44(12), pp. 6235-6243.

Patton, H. et al., 2016. Distribution and characteristics of overdeepenings beneath the Greenland and Antarctic ice sheets: Implications for overdeepening origin and evolution. *Quaternary Science Reviews,* Volume 148, pp. 128-145.

Pattyn, F., 2017. Sea-level response to melting of Antarctic ice shelves on multi-centennial timescales with the fast Elementary Thermomechanical Ice Sheet model (f.ETISh v1.0). *The Cryosphere,* 11(4), pp. 1851-1878.

Pattyn, F., Favier, L., Sun, S. & Durand, G., 2017. Progress in Numerical Modeling of Antarctic Ice-Sheet Dynamics. *Current Climate Change Reports,* 3(3), pp. 174-184.

Pattyn, F., Sun, S. & Simon, E., 2019. Influence of ice-shelf collapse on Antarctic grounding-line dynamics: results from ABUMIP.. *Geophysical Research Abstracts,* 21(1).

Porter, D. et al., 2014. Bathymetric control of tidewater glacier mass loss in northwest Greenland. *Earth and Planetary Science Letters,* Volume 401, pp. 40-46.

Radić, V. et al., 2014. Regional and global projections of twenty-first century glacier mass changes in response to climate scenarios from global climate models. *Climate Dynamics,* 42(1-2), pp. 37-58.

Reynolds, R., Rayner, N. & Smith, T., 2002. An Improved In Situ and Satellite SST Analysis for Climate. *Journal of Climate,* 15(3), pp. 1609-1625.

Rignot, E. et al., 2021. Retreat of Humboldt Gletscher, North Greenland, Driven by Undercutting From a Warmer Ocean. *Geophysical Research Letters,* 48(e2020GL091342).

Rignot, E., Gogineni, S., Joughin, I. & Krabill, W., 2001. Contribution to the glaciology of northern Greenland from satellite radar interferometry. *Journal of Geophysical Research: Atmospheres,* 106(D24), pp. 34007-34019.

Rignot, E. & Kanagaratnam, P., 2006. Changes in the Velocity Structure of the Greenland Ice Sheet. *Science,* 311(5763), pp. 986-990.

Rignot, E. et al., 2014. Widespread, rapid grounding line retreat of Pine Island, Thwaites, Smith, and Kohler glaciers, West Antarctica, from 1992 to 2011. *Geophysical Research Letters,* 41(10), pp. 3502-3509.

Rignot, E., Mouginot, J. & Scheuchl, B., 2011. Antarctic grounding line mapping from differential satellite radar interferometry. *Geophysical Research Letters,* 38(L10504).

Roemmich, D. et al., 2009. The Argo Program: Observing the Global Ocean with Profiling Floats. *Oceanography,* 22(2), pp. 34-43.

Sakakibara, D. & Sugiyama, S., 2019. Seasonal ice-speed variations in 10 marine-terminating outlet glaciers along the coast of Prudhoe Land, northwestern Greenland. *Journal of Glaciology,* pp. 1-10.

Scambos, T. et al., 2009. Ice shelf disintegration by plate bending and hydro-fracture: Satellite observations and model results of the 2008 Wilkins ice shelf break-ups. *Earth and Planetary Science Letters,* 280(1), pp. 51-60.

Schoof, C., 2007. Ice sheet grounding line dynamics: Steady states, stability, and hysteresis. *Journal of Geophysical Research: Earth Surface,* 112(F03S28).

Selmes, N., Murray, T. & James, T., 2011. Fast draining lakes on the Greenland Ice Sheet. *Geophysical Research Letters,* 38(15).

Seroussi, H. et al., 2017. Continued retreat of Thwaites Glacier, West Antarctica, controlled by bed topography and ocean circulation. *Geophysical Research Letters,* 44(12), pp. 6191-6199.

Shabtaie, S. & Bentley, C., 1987. West Antarctic ice streams draining into the Ross Ice Shelf: Configuration and mass balance. *Journal of Geophysical Research: Solid Earth,* 92(B2), pp. 1311-1336.

Shroyer, E., Samelson, R., Padman, L. & Münchow, A., 2015. Modeled ocean circulation in Nares Strait and its dependence on landfast-ice cover. *Journal of Geophysical Research: Oceans,* 120(12), pp. 7934-7959.

Slater, D. et al., 2019. Estimating Greenland tidewater glacier retreat driven by submarine melting. *The Cryosphere,* 13(9), pp. 2489-2509.

Slater, T. et al., 2021. Review article: Earth's ice imbalance. *The Cryosphere,* Volume 15, pp. 233-246.

Smith, B. et al., 2020. Pervasive ice sheet mass loss reflects competing ocean and atmosphere processes. *Science,* 368(6496), pp. 1239-1242.

Solgaard, A. et al., 2020. Hagen Bræ: A Surging Glacier in North Greenland—35 Years of Observations. *Geophysical Research Letters,* 47(e2019GL085802).

Steffen, K., J. E. Box & Abdalati, W., 1996. Greenland Climate Network: GC-Net", in. Colbeck, S. C. Ed. *CRREL 96-27 Special Report on Glaciers, Ice Sheets and Volcanoes, trib. to M. Meier*, pp. 98-103.

Storto, A., Masina, S. & Navarra, A., 2016. Evaluation of the CMCC eddy-permitting global ocean physical reanalysis system (C-GLORS, 1982–2012) and its assimilation components. *Quarterly Journal of the Royal Meteorological Society,* 142(695), pp. 738-758.

Straneo, F. & Heimbach, P., 2013. North Atlantic warming and the retreat of Greenland's outlet glaciers. *Nature,* 504(7478), pp. 36-43.

Straneo, F. et al., 2012. Characteristics of ocean waters reaching Greenland's glaciers. *Annals of Glaciology,* 53(60), pp. 202-210.

Taherkhani, M. et al., 2020. Sea-level rise exponentially increases coastal flood frequency. *Scientific Reports,* 10(6466).

The IMBIE Team, 2020. Mass balance of the Greenland Ice Sheet from 1992 to 2018. *Nature,* 579(7798), pp. 233-239.

Timmermans, M. & Marshall, J., 2020. Understanding Arctic Ocean Circulation: A Review of Ocean Dynamics in a Changing Climate. *Journal of Geophysical Research: Oceans,* 125(e2018JC014378).

Titchner, H. & Rayner, N., 2014. The Met Office Hadley Centre sea ice and sea surface temperature data set, version 2: 1. Sea ice concentrations. *Journal of Geophysical Research: Atmospheres,* 119(6), pp. 2864-2889.

Våge, K. et al., 2018. Ocean convection linked to the recent ice edge retreat along east Greenland. *Nature Communications,* 9(1287).

van Dongen, E. et al., 2020. Numerical Modeling Shows Increased Fracturing Due to Melt-Undercutting Prior to Major Calving at Bowdoin Glacier. *Frontiers in Earth Science,* 8(253).

Vaughan, D., 1994. Investigating tidal flexure on an ice shelf using kinematic GPS.. *Annals of Glaciology,* Volume 20, pp. 372-376.

Vincent, W. & Mueller, D., 2020. Witnessing ice habitat collapse in the Arctic. *Science,* 370(6520), pp. 1031-1032.

Walker, D. et al., 2007. Oceanic heat transport onto the Amundsen Sea shelf through a submarine glacial trough. *Geophysical Research Letters,* 34(2).

Washam, P., Nicholls, K., Münchow, A. & Padman, L., 2019. Summer surface melt thins Petermann Gletscher Ice Shelf by enhancing channelized basal melt. *Journal of Glaciology,* 65(252), pp. 662-674.

Weertman, J., 1974. Stabillity of the Junction of an ice sheet and an ice shelf. *Journal of Glaciology,* 13(67).

Wilson, N., Straneo, F. & Heimbach, P., 2017. Satellite-derived submarine melt rates and mass balance (2011–2015) for Greenland's largest remaining ice tongues. *The Cryosphere,* 11(6), pp. 2773-2782.

Wood, M. et al., 2021. Ocean forcing drives glacier retreat inGreenland. *Science Advances,* 7(eaba7282).

Yamanokuchi, T., Doi, K. & Shibuya, K., 2005. Validation of grounding line of the East Antarctic Ice Sheet derived by ERS-1/1 interferometric SAR data. *Polar Geoscience,* Volume 18, pp. 1-14.

Zuo, H. et al., 2019. The ECMWF operational ensemble reanalysis–analysis system for ocean and sea ice: a description of the system and assessment. *Ocean Science,* 15(3), pp. 779-808.

Appendix

1. Matlab code used to extract average annual ocean temperature means at each study site. Developed from code supplied by Frazer Christie (SPRI – personal comms):

```
%% Clear workspace
clear all; close all;
addpath(genpath('/Directory/Location')); % Change this line to your
data directory
cd('/Directory/Location'); %As above
% MUST install Antarctic/Arctic Mapping toolbox before proceding
with next section of code

%% Mask data
%%Add Region of Interest (RoI) perimeter co-ordinates (Polar
Stereographic) and convert to LL
roi_points = csvread('BOXPMannCoordinates.csv',1,0); %CSV containing
Polar Stereographic co-ordinates of bounding box (If coords in
degrees, this step doesn't need to be run)
[roi_lat, roi_lon] = psn2ll(roi_points(:,1),roi_points(:,2));
%Convert to LL - (psn2ll should be substituted for ps2ll if using
Antarctic Mapping, not Arctic)
clear roi_points

%Load model grid (PS) to find grid cells falling within RoI
perimeter limits
lat = double(ncread('EnsembleMean2016Monthly.nc','latitude'));
lon = double(ncread('EnsembleMean2016Monthly.nc','longitude'));
[lati, loni] = meshgrid(lat,lon);
[maskin, maskout] = inpolygon(lati,loni,roi_lat,roi_lon);

%Generate logical mask containing RoI grid cells
masknan_in = double(maskin); %Logical values (1,0) cannot be
converted to NaN, but doubles can.
masknan_in(masknan_in==0) = NaN; %Convert zeroes to NaN.

%Load model data, and clip to mask limits
T = ncread('EnsembleMean2016Monthly.nc','thetao_mean');
T = T.*masknan_in; %Multiplies m*n-sized (2D) mask with m*n*d (3D)
array.

% Load additional model data
depth = ncread('EnsembleMean2016Monthly.nc','depth');
time = ncread('EnsembleMean2016Monthly.nc','time'); %Load time

%% % Calculate monthly average of deep/surface waters **Change
Depths as appropriate**

TmeanMonthly = mean(T(:,:,1:31,:),3,'omitnan'); %Average of
deep/surface waters (edit depth layer range as appropriate for
incremental runs)
size(TmeanMonthly) %Check size of output
```

```
%% Calculate annual average temperature of each pixel within study
box
TmeanAnnual = mean(TmeanMonthly(:,:,:,1:end),4,'omitnan'); %Then,
average this over all times
size(TmeanAnnual) %Check size of output

%% Plot figure to check data **Change Title as appropriate**
figure;
title('Annual Average Ocean Temperature – Petermann 2016');
LatLim = [75 85]; %Define map lat limits
LonLim = [-70 -10]; %Define map lon limits
h = worldmap(LatLim,LonLim); %Tell figure to be a map, with limits
as prescribed above
surfm(lat,lon,TmeanAnnual(:,:,1,1)');
hold on
bordersm('countries','facecolor',[0.5 0.5 0.5]);
caxis([-1.5 1.5]);
colorbar
plotm(roi_lat,roi_lon,'linewidth',2,'color','r') %Plot bounding box
limits

%% Calculate mean of all cells in study area
%Now, calculate mean of all cells in the ROI
Tmean_StudyArea = mean(TmeanAnnual(:),'omitnan') %Returns mean of
all lats, all longs
```

2. Matlab code used to extract and plot increase in local temperature surrounding North Greenland at surface and deep waters. Developed from code supplied by Frazer Christie (SPRI – personal comms):

```
clear all; close all; % clear all variables and figures

%Change directory and add path to data
cd('/Directory/Location'); %edit to point to your own directory
addpath(genpath('/Directory/Location')) %as above


%% Load data
ncdisp('EnsembleMean1995Monthly.nc') %First, display contents of nc
file to get variable names

lat = double(ncread('EnsembleMean1995Monthly.nc','latitude')); %Load
lat
lon = double(ncread('EnsembleMean1995Monthly.nc','longitude'));
%Load lon
depth = double(ncread('EnsembleMean1995Monthly.nc','depth')); %Load
pot. temp.
temp95 = ncread('EnsembleMean1995Monthly.nc','thetao_mean'); %Load
pot. temp.
time = ncread('EnsembleMean1995Monthly.nc','time'); %Load time
```

```
%% Load data
ncdisp('EnsembleMean2016Monthly.nc') %Display contents of nc file to
get variable names

temp16 = ncread('EnsembleMean2016Monthly.nc','thetao_mean'); %Load
pot. temp.

%% Calculate mean of all months between 1 and 12 inclusive

annual_mean_temp_1995 = mean(temp95(:,:,:,:),4,'omitnan');
annual_mean_temp_2016 = mean(temp16(:,:,:,:),4,'omitnan');


%% Calculate mean of all surface waters (depths between level 1 and
31 inclusive (0-199.79 mbsl)),

surface_waters_1995 =
mean(annual_mean_temp_1995(:,:,1:31),3,'omitnan');
surface_waters_2016 =
mean(annual_mean_temp_2016(:,:,1:31),3,'omitnan');

%% Ccalculate mean of all depths between level 31 and 44 inclusive
(199.79-773.36 mbsl),

deep_waters_1995 =
mean(annual_mean_temp_1995(:,:,31:44),3,'omitnan');
deep_waters_2016 =
mean(annual_mean_temp_2016(:,:,31:44),3,'omitnan');

%% Calculate difference between start and end year average
temperature

deep_increase = deep_waters_2016-deep_waters_1995;
surface_increase = surface_waters_2016-surface_waters_1995;


%% Check data can be plotted

imagesc(lat,lon,surface_increase);
imagesc(lat,lon,deep_increase);

%% Plot deep ocean temperature increase over study period
grey = [225 235 221]./255; %custom colour definition (numbers in []
correspond to RGB values)
LatLim = [78 86]; %Define map lat limits
LonLim = [-70 0]; %Define map lon limits
figure; %Generate figure
set(gca,'FontSize',18);
h = worldmap(LatLim,LonLim); %Tell figure to be a map, with limits
as prescribed above
surfm(lat,lon,deep_increase'); %Plot data
hold on
bordersm('countries','facecolor',grey,'edgecolor','none'); %
'borders' function
(https://uk.mathworks.com/matlabcentral/fileexchange/50390-borders)
to add countries. These are higher resolution than MATLAB default
c = colorbar;
```

```
c.Label.String = '(\circC)';
setm(gca,'mlinelocation',10)
setm(gca,'mlabellocation',10)
cmocean('balance','pivot'); %cmocean provides colourmaps for ocean
data. (https://uk.mathworks.com/matlabcentral/fileexchange/57773-
cmocean-perceptually-uniform-colormaps)
caxis([-1 1.5]);
title('Deep ocean temperature increase (\circC) 1995-2016');
axesm;

%% Plot surface ocean temperature increase over study period
grey = [225 235 221]./255;
LatLim = [78 86];
LonLim = [-70 0];
figure;
set(gca,'FontSize',18);
h = worldmap(LatLim,LonLim);
surfm(lat,lon,surface_increase');
hold on
bordersm('countries','facecolor',grey,'edgecolor','none');
c = colorbar;
c.Label.String = '(\circC)';
setm(gca,'mlinelocation',10)
setm(gca,'mlabellocation',10)
cmocean('balance');
caxis([-1.5 1.5]);
title('Surface ocean temperature increase (\circC) 1995-2016');
axesm;
```